Dissecting kinetic differences in acetylcholine receptors incorporating an ancestral subunit.

Christian Tessier

Thesis submitted to the

Faculty of Graduate and Postdoctoral Studies

in partial fulfillment of the requirements for the
Master's degree in Chemistry

Department of Chemistry and Biomolecular Sciences
Faculty of Science
University of Ottawa

Candidate	Supervisor
Christian Tessier	Professor Corrie daCosta

ABSTRACT

At the neuromuscular junction, nicotinic acetylcholine receptors (AChRs) convert chemical stimuli into electrical signals. They are heteropentameric membrane protein complexes assembled from four evolutionary related subunits (two α subunits, and one each of the β-, δ-, and ε-subunits), arranged around a central ion-conducting pore, which is regulated by the neurotransmitter acetylcholine. Understanding how the binding of acetylcholine leads to channel opening is of fundamental importance. While it is known that channel opening results from a global conformational change involving the cooperative action of all five subunits, how the subunits achieve this cooperativity is unclear. Our hypothesis is that this subunit cooperation is maintained through coevolution of the subunits, and thus studies of subunit coevolution can provide insight into subunit cooperativity. Using an ancestral reconstruction approach, combined with single-molecule patch clamp electrophysiology, we have begun dissecting the mechanistic consequences of preventing coevolution of the acetylcholine receptor β-subunit. This approach has allowed us to identify new amino acid determinants of acetylcholine receptor function.

ACKNOWLEDGEMENTS

I would like to thank Professor Corrie daCosta for the opportunity to join and work in his research group, and for taking me on as his first graduate student. Through the work that I completed in the lab, I gained lots of scientific knowledge, the most important thing being learning the technicalities involved in electrophysiology and single molecule experiments. I would like to thank all the supportive people who have helped me complete my research at the University of Ottawa. I would also like to thank Professor Natalie Goto and Professor John Baenziger for agreeing to be on my evaluation committee and for their guidance. Finally, I would like to thank the funding agencies that allowed this research to happen, most importantly the University of Ottawa.

TABLE OF CONTENTS

LIST OF FIGURES AND TABLES

LIST OF ABBREVIATIONS

5-HT3	5-hydroxytryptophan (Serotonin)
Å	Ångström
ACh	Acetylcholine
AChBP	Acetylcholine Binding Protein
alRT	approximate likelihood Ratio Test.
βAnc	Ancestral beta subunit
Cryo-EM	Cryo-Electron Microscopy
EC50	Concentration at 50% maximum effect
ELIC	*Erwinia chrysanthemi* ion channel
GABA	Gamma-Aminobutyic Acid
GFP	Green Fluorescent Protein
GLIC	*Gloeobactor violaceus* Ligand Gated Ion Channels
HEK293	Human Embryonic Kidney Cells
kDa	KiloDalton
kHz	KiloHertz
LBD	Ligand Binding Domain
M	Molarity
M1	1^{st} transmembrane spanning segment of nAChR
M2	2^{nd} transmembrane spanning segment of nAChR
M3	3^{rd} transmembrane spanning segment of nAChR
M4	4^{th} transmembrane spanning segment of nAChR
MA	α- helix of intracellular domain of nAChR
mV	milliVolts
ms	milliseconds
μM	microMolar
μs	microseconds
MWC	Monad-Wyman-Changeux
NNI	nearest neighbour interchange
Ω	Ohms
pA	picoAmperes
pLGIC	pentameric Ligand Gated Ion channel
pOpen	Open probability
SH	Shimodaira-Hasegawa
SPR	subtree pruning and regrafting
τ_{crit}	critical closed duration
WT	Wild Type

CHAPTER 1.0: INTRODUCTION AND LITERATURE REVIEW

1.1 Ion channels

Ions are unable to pass through hydrophobic lipid bilayers. To solve this problem, cells have evolved ion channel proteins to conduct ions across their membranes. Ion channels are usually formed from multiple protein subunits arranged around a central ion-conducting pore.[1] The number of subunits varies across different ion channel types. Subunits can either be identical (homomeric channels) or homologous (heteromeric channels)[2]. Adding to this complexity, different channels are gated open and closed by diverse stimuli, such as transmembrane voltage, mechanical stress, or the binding of small chemical ligands[3-5]. Due to their ability to transmit electrical signals, ion channels have important physiological roles and are considered promising drug targets[6,7]. Thus understanding ion channel structure and function is not only important for a molecular description of human physiology, it is immediately relevant to human health.[8]

1.2 Pentameric ligand gated ion channels

Opened by the binding of small molecule agonists, ligand-gated ion channels convert chemical signals into electrical impulses[9]. There are many different ligand-gated ion channel types distinguished by their agonist specificity, ion selectivity, and oligomeric structure[10]. Formed from five homologous or identical subunits arranged around a central pore, pentameric ligand gated ion channels (pLGICs) are the largest and most structurally diverse family of ligand-gated channels. [10-13]

Most famous for mediating neurotransmission in the mammalian nervous system, pLGICs are found in almost all forms of life, including bacteria[9,14]. Eukaryotic pLGICs were originally

termed "cys loop" receptors because they are distinguished by a stretch of 13 amino acids flanked by two cysteine residues that form a disulfide bond. This eponymous "cys loop" is highly conserved and functionally important[15]. Mammalian cys loop receptors can be selective for either positively or negatively charged ions[16,17]. Anion specific receptors, gated by either GABA or glycine, conduct negatively charged ions and result in inhibitory responses[18,19]. Cation selective channels, such as those gated by 5-HT_3 and acetylcholine, transport sodium and potassium and result in an excitatory response[2,20].

Due to the ease of expression and isolation, prokaryotic homologues of the eukaryotic Cys loop receptors have been pivotal to our understanding pLGIC structure. The x-ray structures of two bacterial pLGICs in particular, ELIC and GLIC, originating from *Erwinia chrysanthemi* and *Gloeobacter violaceus* respectively, have been solved under a number of different conditions [21-24]. In addition, the molluscan acetylcholine binding proteins (AChBPs), soluble homopentameric homologs of the acetylcholine receptor extracellular ligand binding domain, have also provided high resolution insight into the acetylcholine receptor ligand-binding domain[25,26]. Molluscan AChBPs and bacterial pLGICs, combined with continued improvement of cryo-electron microscopy of the AChR from the electric organ of *Torpedo marmorata*, have led to a detailed picture of the architecture and structure of pLGIC superfamily of receptors. With advancement in cryo-electron microscopy (cryoEM) technologies, attempts to use these methods on ion channels, has yielded substantial information of the AChR structure[27]. In 2012, using cryoEM, both open and closed AChR conformations were captured, providing insight into the gating movement of the protein[28]. More recently, crystal structures have emerged for the neuronal α4β2 acetylcholine receptor and of the GABA receptor [29,30]. Both of these structures provide insight into structural characteristics of all pLGIC due to their similar evolutionary origins.

1.3 Acetylcholine receptors

There are 16 evolutionarily related mammalian nicotinic acetylcholine receptor (AChR) subunits: nine α-, four β-subunits, as well as one each of the ϵ-, δ-, and γ-subunits. α-subunits are distinguished by the presence of two adjacent cysteine residues that form a vicinal disulphide bond[31]. The remaining subunits have been named based on their relative date of discovery or their homology to the original β1-subunit[32]. Some α-subunits can self-assemble, forming homopentamers, while others combine with various β-subunits, or in the case of the muscle AChR the remaining accessory subunits to form heteropentamers. The most complex subunit combination is found at the neuromuscular junction, where muscle-type acetylcholine receptors contain two α_1 subunits, with a β_1-, a δ-, and an ϵ-subunit[2].

Acetylcholine receptors are present throughout the body with high concentrations in the nervous system[14]. Altered cholinergic signaling has been linked to a multitude of human diseases including: Alzheimer's, epilepsy, and Parkinson's[33-35]. Nicotinic acetylcholine receptors in the brain are also the targets for exogenous nicotine, and mediate nicotine addiction[36]. Acetylcholine receptors are thus considered promising drug targets for the treatment of a variety of diseases, as well as addiction. Unfortunately, the high homology of different acetylcholine receptor types makes selective targeting of different subtypes difficult.[37] Understanding structure-function relationships that orchestrate the opening of the ion channel provide insight into improved target strategies.

1.4 Acetylcholine receptor structure

Early structural studies of acetylcholine receptors revealed densely packed rosettes, which appeared as 80Å wide cylindrical rods, projecting perpendicular to the cell membrane.[38] Spanning the membrane, the rods also had both intracellular and extracellular projections.[39] With a molecular weight of 250kDa for the full pentamer, individual subunit molecular weights were determined by gel electrophoresis, with a 40kDa protein band corresponding to the α subunit, a 50kDa band for the β subunit, a 60kDa band for the γ subunit, and a 65kDa band for the δ subunit[40]. Densitometry of the gels also suggested that two α subunits were present for each copy of the other subunits. *Torpedo* and fetal muscle-type heteropentamers adhere to a strict subunit arrangement of α – γ – α – δ – β, in a counterclockwise rotation (Figure 1A) [28]. Whereas, the adult muscle type acetylcholine receptor, incorporates the ε subunit in place of the γ subunit, which occurs during development[41]. The discovery of the soluble acetylcholine binding proteins in snails, and their subsequent x-ray structure determination, combined with continued improvements in cryo-electron microscopy, provided a seminal 4 Å resolution structure of the *Torpedo* acetylcholine receptor allowing placement of almost all the atoms in the pentamer structure with the exception of ~100 residues within the intracellular domain (Figure 1A/B)[25,27].

The refined 4 Å structure of the protein provided insights into intra-subunit and inter-subunit protein interactions[27]. Structurally, each acetylcholine receptor subunit can be divided into three domains: extracellular, transmembrane and intracellular domains[27]. Two functionally important sites within the pentamer can be distinguished; the ligand binding site(s) and the ion-conducting pore.

The extracellular domain of each acetylcholine receptor subunit is composed of one α helix and ten β strands. These 10 β strands are distributed between an inner and an outer β sheet[1,42]. The outer β sheet, formed by 4 β strands, forms the peripheral face of the extracellular domain, where interactions with ligands and allosteric molecules occur. (Figure 1C) The 6 remaining β strands form the inner sheet which lines the ion-conducting pore. Structurally these β strands are connected with varying lengths of linkers, which play important roles in signaling throughout the pentamer. More specifically, the β6-β7 linker of the extracellular domain pertains to the Cys-loop, which is responsible in the communication between the ligand binding domain and the pore[43].

The AChR transmembrane domain is composed of four α helices that span the membrane denoted: M1, M2, M3, and M4. The M1 and M3 helices interact with the transmembrane domains of adjacent subunits[44]. The M4 helix is most distal to the pore and interacts with surrounding lipids in the membrane[45]. The M2 helix projects inwards to the ion-conducting pore, and is responsible for opening and closing the pore[46]. The linkers connecting M1-M2 and M3-M4 project intracellularly contributing to the cytoplasmic domain, where ~100 residues of the intracellular domain remain missing from crystal structures[47]. The M2 helix projects residues into the ion-conducting pore. These residues are responsible for interacting with ions, and impart a selectivity filter for the flux of cations[48,49]. Overall, these pore lining residues of the M2 have a great influence on ion channel conductance and kinetics[50,51].

The AChR intracellular domain of each subunit is composed primarily by the residues linking the M3-M4 helices, for which little structural information is known. Approximately 100 amino acid residues within the intracellular domain remain excluded from the crystal structures due to the inability detect accurate structural models of these residues. This could be due to the intracellular domain adopting a disordered or static conformation, impinging on the ability to

acquire accurate structural models. Each of the acetylcholine receptor subunits contains variability in sequence and in length within this region. Despite advancements in cryoEM, the intracellular region of the AChR remains the least characterized structural domain[52].

The extracellular ligand binding domain (LBD) of the AChR is nestled between adjacent subunits[26,53]. The muscle-type AChR contains two ligand binding sites located at the interface of the $\alpha - \epsilon$ and $\alpha - \delta$ subunits (Figure 1A). Acetylcholine (ACh), the endogenous ligand, and other agonists bind at both binding sites to elicit opening of the ion channel. The binding site is made up of seven strategically oriented loops, each contributing important residues that stabilize binding of the agonist molecule. Acetylcholine is stabilized in the agonist binding site through interactions between acetylcholine's charged amine group and the surrounding aromatic residues. The principle (+) side of the binding site, is always contributed by the α subunit, while the accessory subunit provides the complementary (-) side of the binding site. Loops A, B and C are contributed by the α subunit, while loops D, E, F and G are contributed by either the δ- or the ϵ/γ subunit[5,26]. Once an agonist molecule enters the ligand binding site, a conformational change of these 7 loops is triggered, leading to a global conformational change which opens the ion-conducting pore.

The AChR ion-conducting pore allows flux of ions through the membrane and into cells. When the pore is closed, the backbone of the M2 helices are kinked inward obstructing the flow of ions. Upon opening of the pore, the M2 helices are retracted allowing for the passage of ions[54]. The opening of the pore is mediated through specific rings, comprised of homologous residues on each of the five subunits, along their M2 helices. The widest portion of the pore is at the extracellular lumen, while the narrowed section is at the midsection of the transmembrane domain. Findings in the late 1980's and early 1990's by Imoto et al. provided insight into important residues lining the ion channel pore. Four important rings of residues were identified[55,56]. Each of these

rings are made up of one residue from each of the five subunits in the pentamer. The internal, intermediate and external rings are placed accordingly throughout the pore lining M2 helix. Composed of negatively charged amino acids, these three rings locally concentrate cations, thereby playing a role in ion selectivity. The fourth ring, discovered subsequently, is referred to as the central ring and composed of five uncharged residues[57]. The central ring sits three residues downstream of the intermediate ring. All four of these rings impart function in regulating the ion concentrations, and interact with passing ions, imparting their potential effect on conductance.

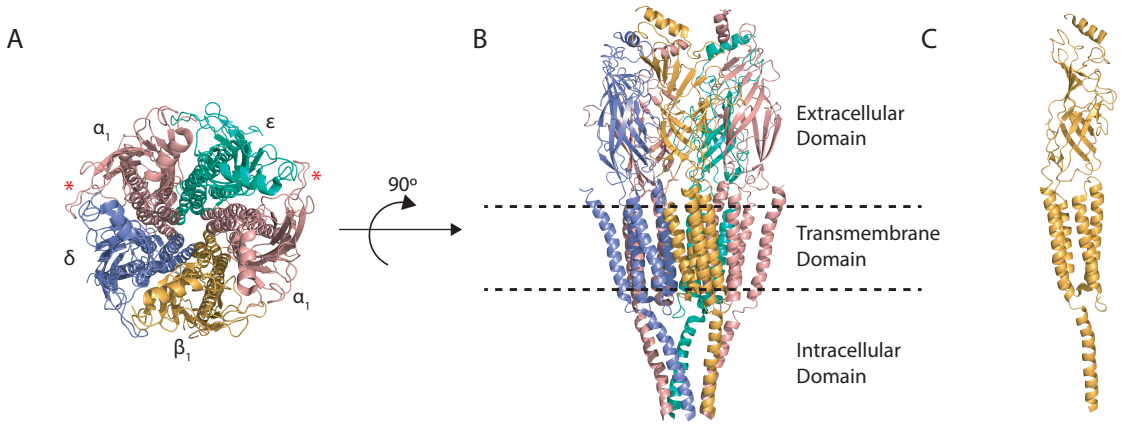

Figure 1: Muscle-type acetylcholine receptor heteropentamer (A/B) and individual subunit (C) structure.
(A). Extracellular view of muscle-type acetylcholine receptor, 5 homologous subunits (2α, β, δ, and ε) encircle the ion conducting pore. Agonist binding sites are present at the α-ε and α-δ interfaces, denoted by *. (B) View of acetylcholine receptor through the plane of the cellular membrane. Receptors are subdivided into three structural domains; extracellular, transmembrane and intracellular. (C) Individual acetylcholine receptor subunit. Structural diagrams obtained from PDB: 2BG9; *Torpedo* AChR at 4Å resolution.

1.5 Techniques to study ion channels

Early experiments on excitable membranes, including those of Hodgkin and Huxley in the 1950s, measured the electrical potentials of giant squid axons[58]. What they were actually measuring was electric current, generated from ion flux through ion channels. Building upon these early studies, the idea of discrete sites within the cell membrane that are responsible for regulating ion conductance emerged. These findings translate to modern day knowledge of ion channels, ion selectivity and the role of proteins in electrical conduction. Performing research on ion channels was limited to the techniques and their resolutions at hand, and the affordability of performing such sensitive experiments[1].

It wasn't until the invention of the patch clamp and the first single-channel recordings by Neher and Sakmann in 1976, that the visualization of individual ion channel activity was made possible [59]. The patch clamp technique allowed for single-channel recordings, and also macroscopic recordings via whole cell voltage clamping at a much more sensitive scale. The single-channel patch clamp technique involves a fire-polished glass pipette, containing an electrode. The pipette is used to form a giga-ohm seal with a patch of cell membrane[60]. A second reference electrode is present within the solution bathing the cells. Once the membrane is sealed with the pipette, the user then "clamps" the voltage. 'Clamping' the voltage, a responsibility of a patch clamp amplifier, maintains the voltage to a constant parameter, despite the current changing based on the opening and closing of the ion channel. The researcher then is able to observe through an oscilloscope, the rapid channel openings and closing through the patch clamp, as the amplifier detects the changes in current as the channel opens and closes. This data can then be digitally stored so kinetic analysis of the single-channel data can be performed. The patch clamp technique has allowed researchers to identify functionally important residues present within ion channels.

Stochastic kinetic models have been used to gain insights into the channel gating mechanism and how the protein changes from the closed to opened states[61]. Single-channel data is rich with kinetic information making it possible to uncover different states of dynamic ion channels.[62]

1.6 Ion channel states: open, closed and blocked

According to the classic del Castillo-Katz scheme (Scheme I) first proposed in 1957, activation of the AChR can be separated into two discrete steps: agonist "binding" and channel "gating"[63]. The binding step relates to the reversible association between the receptor and an agonist molecule. Once binding is complete, the ion channel remains in a non-conducting closed state[43]. The proceeding step to opening the ion channel, gating, results from a conformational change discrete from agonist binding[28,64,65]. The global conformational change of the gating reaction is a result of movement within the five subunits that results in the widening of the pore to allow for ion flux. Due to the presence of two binding sites present in the muscle type acetylcholine receptor, the del Castillo and Katz scheme has been expanded to consider mono-liganded and di-liganded channel openings.

Scheme I:

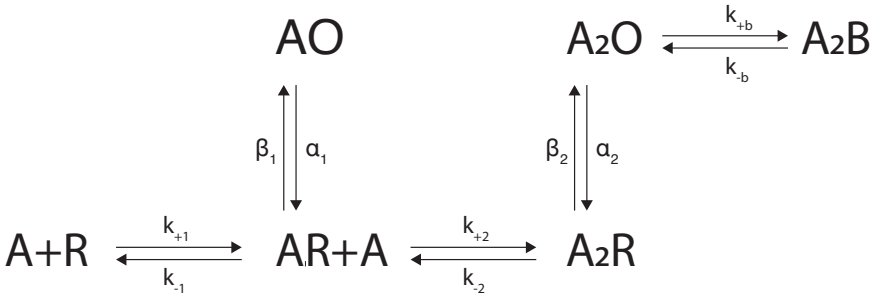

In this scheme, ‘R’ is the resting conformation of the receptor, ‘O’ is the open conformation of the receptor, and ‘B’ corresponds with the non-conducting blocked channel state. ‘A’ refers to the agonist molecule (i.e. acetylcholine), where k_{+1} and k_{+2} are concentration dependent binding rates, and k_{+b}, corresponds to the concentration depending blocking rates. k_{-1}, k_{-2}, and k_{-b} all denote unbinding events, which are not concentration dependent. β_1 and β_2 correspond to channel opening rates, while α_1 and α_2 represent the channel closing rates.

Agonists of nicotinic receptors are notorious for not only activating channel opening, but also physically occluding the open channel pore at higher agonist concentrations[66,67]. Open channel block by charged agonists is further exacerbated by increased transmembrane voltage, thus the need for an additional state was included in the del Castillo and Katz kinetic scheme[66,68]. Blocking of the ion channel by agonist molecules occurs when the agonist molecule enters the pore of the channel and blocks the flow of ions, appearing as if the ion channel is briefly closed. For this reason, an additional non-conducting state is included in the kinetic scheme, referred to as a blocked state, which is connected to the doubly liganded open state[67,69]. This blocked state is agonist concentration dependent, and reversible upon removal of the agonist molecule from the pore. Mono-liganded openings are too brief to exhibit substantial block and thus, it is not of significant prevalence to include an additional state in the kinetic scheme.

Due to the complexity of AChRs, additional states in kinetic schemes have been included to take into account different protein states. These additional states include additional intermediate conformations which are not included in the classic del Castillo and Katz kinetic model. These higher order schemes, with intermediate closed states include, the Monad-Wyman-Changeux model (MWC)[70], the flipped model[71], and the priming model[72].

An insight, built upon the classic del Castillo and Katz mechanism, was brought forth with the finding of the desensitized state[73,74]. The desensitized state is a non-conducting state, that forms after many successive channel openings, manifesting as with extended quiescent periods. The identification of this refractory state led to the hypothesis of higher agonist affinity for desensitized receptors, relative to that of resting state. To explain this, Katz and Thesleff proposed a cyclic mechanism similar to the MWC model, taking into account the desensitized state[73]. Unfortunately, this cyclic scheme required the observation of unliganded openings, which are not of high prevalence in AChRs.

Neither the MWC or the flip mechanism could explain the presence of long lived channel openings, or the presence of multiple exponential components of unliganded channel openings observed in some AChR pore mutants with measurable spontaneous opening events. [70,75]. In these mutants, open and closed dwell time histograms displayed multiple exponential components, which can be accounted for by closed primed states, that are adopted before the channel can open. In this model, each of the primed states corresponds to a change in the agonist binding site, with singly primed receptors eliciting brief openings, and doubly primed receptors giving rise to longer lived openings. The primed mechanism, proposed in 2009, depicts the priming of the agonist binding sites as sequential steps, rather than concerted, as proposed by the MWC and Flip mechanisms[72].

1.7 Evolutionary biochemistry

Ancestral sequence reconstruction (ASR) holds great promise for uncovering structure-function relationships in families of homologous proteins [76,77]. The pLGIC superfamily is largest, and most structurally and functionally diverse family of ligand-gated ion channels [10,12,78]. Composed of five homologous, and thus evolutionarily related subunits, they

represent prime candidates for an ASR approach. As a proof of concept our lab previously reconstructed the sequence of the muscle-type AChR β-subunit. We chose the β-subunit for two reasons. First, it is the least conserved of the four AChR subunits, and so represents the most rigorous challenge to an ASR approach. Second, the β-subunit is the only subunit that does not participate directly in agonist binding. Leaving the agonist/antagonist binding sites intact allowed us to measure cell-surface expression of hybrid acetylcholine receptors containing the ancestral subunit using a radiolabelled antagonist.

Ancestral sequence reconstruction of the ancestral β subunit began by searching the NCBI databank for homologous protein sequences to the *Homo sapiens* β_1 subunit. Initially 116 orthologous sequences were obtained, and aligned with MUSCLE, where sequences containing insertions or deletions were removed[79]. The resulting 60 sequences were combined with 5 homologous outgroup nematode sequences, acting as an evolutionary reference. The 65 sequences were re-aligned with PRANK [80,81] and analyzed in ProtTest to determine the best-fit evolutionary model[82]. PhyML3.0 used the obtained model to infer the maximum likely tree topology, branch lengths and model parameters[83-85]. Within the PhyML software, topology optimizations were completed, including subtree pruning and regrafting (SPR), nearest-neighbor interchange (NNI) and SH-like approximate likelihood ratio tests (aLRT SH-like), to infer phylogeny. Lazarus was then used to infer ancestral sequences and posterior probability distributions of each site, and parsimoniously inserts gaps within the alignments according to the Fitch algorithm[77,86].

The ancestral β-subunit DNA coding sequence was built upon the *Homo sapiens* AChR β1-scaffold. The DNA sequence was built by maintaining the WT sequence at analogous sites, introducing mutations according to the sequences of closely related extant species. The *Homo*

sapiens β1 signal peptide was added to flank the N-terminus of the ancestral β subunit. Additional overhangs were designed to allow for Gibson cloning into the multiple cloning site (MCS) of the pRBG4 vector. The adapted ancestral sequence was purchased as a synthetic construct, cloned and sequence verified. Due to the historical significance of the *Torpedo* AChR, the initial report, reconstructed the last shared common ancestor between *Homo sapiens* and *Torpedo marmorata*, which was called βAnc81. The inferred ancestral sequence does not represent an *exact* ancestor, but instead is a representative member of an entire population of AChRs that existed within an ancestral species that lived ~430 million years ago[87].

Despite 132 mutations distributed throughout the protein, co-expression of the ancestral construct with human subunits (α, δ and ε) resulted in functional acetylcholine receptors. These hybrid AChRs containing the ancestral β-subunit ($\beta_{Anc}81$), formed a complex with the *Homo sapiens* native α, δ, and ε subunits, displaying both altered single-channel conductance and kinetics. [87] The initial report did not examine the underlying mechanistic basis for the observed differences in single-channel kinetics. This is precisely the gap that this thesis aims to fill.

CHAPTER 2.0: OBJECTIVES

2.1 Approach

Using an evolutionary biochemistry approach, the ancestral $\beta_{Anc}81$ sequence was generated (see Prinston et al.)[87]. In order to investigate the mechanistic differences in the observed kinetic change, we take advantage of single-channel patch clamping. Performing patch clamp experiments on ion channels containing the ancestral protein will provide insight into the mechanistic differences in the binding and apparent gating steps of the kinetic scheme. Further experiments will aim to discover the residues that are causing the changes within the ancestral subunit attributed to the change in kinetics, and conductance.

2.2 Experimental design

Using single-channel patch clamping, dose responses ranging from 3μM to 300μM acetylcholine will be used to interrogate the kinetics of the ion channels. Utilizing the evolutionary tree generated in Prinston et al., the sequences of successive ancestors will be used to narrow down residues that are responsible for the change in kinetics. [87]

2.3 Hypothesis

Previously published work provided evidence that the $\beta_{Anc}81$ containing receptors resulted in altered conductance and kinetics of the ion channel, along with a shift in the EC50. Based on the placement of the β subunit within the heteropentamers, and the fact that it does not structurally contribute to the agonist binding site, we hypothesize that the apparent gating step of the del

Castillo and Katz kinetic mechanism will be altered. We expect that the binding kinetics of the ion channel will be minimally altered, due to the unchanged structure of the agonist binding sites.

2.4 Summary of goals and objectives

The goal of our work was set to determine the mechanistic differences in the altered kinetic profile of $\beta_{Anc}81$ containing receptors. Full agonist dose responses will be completed of receptors containing wild-type, or the ancestral version of the β subunit, to determine changes in binding and apparent gating steps. Secondly, potential residues that are responsible for the altered kinetics can be narrowed to a smaller subset of residues, using successive ancestral protein sequences along the evolutionary trajectory.

CHAPTER 3.0: MATERIALS AND METHODS

3.1 Ancestral sequence reconstruction

Ancestral sequence reconstruction of $\beta_{Anc}81$ subunit, and phylogenetic tree construction is described in detail in Prinston et al. [87].

3.2 Sequence reconstruction – generation of mutants

DNA coding sequences corresponding to the investigated nodes in the evolutionary tree, ($\beta_{Anc}81$ $\beta_{Anc}84$, $\beta_{Anc}85$ and $\beta_{Anc}86$) were built using the mammalian β1 background with introduced mutation of DNA sequences according to most frequently used mammalian codons for the targeted amino acid. For both ancestral proteins, the native β1 signal peptide of the human sequence was flanked to the N terminus of the ancestral sequence. An additional 15-20 base overlap homologous to the multiple cloning site were added to both the 5' and 3' termini of the ancestral DNA sequences. The final ancestral subunit constructs were synthesized (gBlock from Integrated DNA Technologies) and subsequently cloned via Gibson Assembly Reaction (New England Biolabs) into the pRBG4 expression vector.

Both single point mutants were generated via site directed mutagenesis. Primers were designed to incorporate the appropriate mutation (2' or 6' mutation). Amplification (ThermoFisher Platinum Superfi), phosphorylation (NEB Polynucleotide Kinase), ligation (NEB T4 DNA ligase), and sequence conformation resulted in both 2' and 6' single mutants. The sequences of all constructs used in this study were verified (Génome Québec).

3.3 Tissue culture

Ion channel expression, and patch clamp experiments were completed on BOSC23 cells, which are modified HEK293 cells [88]. Cells were maintained Dulbecco's modified Eagle's medium (DMEM) containing 10% V/V of fetal bovine serum, and 100 μ/mL penicillin and 100μg/mL of streptomycin. Cells growth was maintained at 37°C under 5% carbon dioxide to a confluency of 70-80%.

3.4 Transfection/mammalian cell expression

Cells were transiently transfected with a combination of α, β, δ, and ϵ subunit cDNAs in the mammalian expression vector, pRBG4. A fluorescent marker, Green Fluorescent Protein(GFP), was also co-transfected to facilitate the identification of transfected cells. Transfections were completed out using a calcium phosphate mediated transfection for between 2-5 hours with varying recovery time based on required protein expression. Transfection reactions were quenched by changing the culture medium.

3.5 Electrophysiology

Single-channel patch clamp recordings were performed as described previously [89]. Patch clamp recordings were performed on transiently transfected BOSC cells, with the combination of α, β, δ, ϵ, and GFP subunits. Recordings were obtained using a cell attached patch clamp configuration with a membrane potential of -120mV, and a room temperature of 19-22°C. External bath solution contained 142mM KCl, 5.4mM NaCl, 0.2mM $CaCl_2$, and 10mM HEPES, which was adjusted to a pH of 7.4 with KOH. The internal pipette solution contained 80mM KF, 40mM K-Aspartate, 20mM KCl, 10mM HEPES, 2mM $MgCl_2$ and 1mM EGTA, adjusted to pH 7.4 with

KOH[72,90]. Acetylcholine was added to the internal pipette solution to the respective range of concentrations through serial dilution (3μM, 6μM, 10μM, 18μM, 30μM, 60μM, 100μM, 180μM and 300 μM) for dose response characterization of mutants

Patch pipettes were fabricated from type 7052 non-filamented glass capillaries (King Precision Glass), with inner diameter of 1.15mm and outer diameter of 1.65mm. Capillaries were pulled with a horizontal puller (Sutter Instruments P-1000) tapered to a final pipette opening of 1-2μm. Pipettes were coated with SYLGARD 184 (Corning), and heat polished to a final resistance of 5 to 8Ω.

Single-channel currents were recorded from an Axopatch 200B patch clamp amplifier with a gain of 100mV/pA and an internal Bessel filter set to 100kHz. Using a data sampling interval of 1μs and a BNC-2090 Analog to Digital converter with a PCI6111e acquisition card, data was recorded using the program Acquire (Bruxton).

3.6 Single-channel analysis

Single-channel analysis was completed using a 50% threshold detection software, TAC (Bruxton). Using a 50% threshold provides an equivalent probability of missing brief opening and brief closing event [91], [92-95]. All data was digitally filtered using a Gaussian filter set to 10kHz within TAC, and channel amplitude was determined from activity within each recording. All points histograms provided Gaussian distributions of the baseline and open channel conductance, from the mean of 15 segments of activity the unitary current amplitude was obtained. Threshold detection was completed with a threshold at 50% of the unitary conductance. Data was analyzed with the exclusion of any set of activities with two channels present, and activity with only one opening present were also excluded. Dwell times were corrected for the filter frequency and placed

into open and closed dwell time histograms, where the distributions of each histograms were fit by a sum of exponentials.

3.7 Data correction

3.7.1 Digital filter correction

The data corrections of the single-channel recordings were completed in R (R Project for Statistical computing). All recordings were first corrected for the limit of the machine, and the time it takes to react to the opening of the channel, this value is based on machine used, and is known as the risetime. Corrections also took into account an aliasing introduced by the 10kHz digital filter, and corrected for the signal disruption. [96]

3.7.2 Burst definition – critical closed duration

Since analysis is restricted to single-channel activity, bursts were identified as clusters of openings in a closely spaced event flanked by closings longer than a critical closed time(τ_{crit}). The τ_{crit} was calculated based on the intersection of two exponential components, corresponding to the longer lived closed states, within the closed time histogram.

3.7.3 Determine normality of burst pOpen

The probability of being open for each segment of activity within a recording (pOpen) was plotted in a histogram, which resulted in a normal distribution, albeit with outliers that were later removed. Bursts that contained 1 opening and closing were removed, since no kinetic variables

can be obtained from this type of burst. Each of the recordings were fit with an overlay of a Gaussian distribution, provided in a package in R. (R packages: ggplot, MASS, grid, gridExtra)

3.7.4 Removing non-normally distributed bursts

For each of the recordings, a Normality test (R package: extremevalues [97]), present as a package in R was used to mathematically determine outliers from the normally distributed data.[97] Outliers were removed based on this statistical test and subsequently the mean and standard deviation of the normally distribution data was obtained.

3.7.5 Removing data beyond two standard deviations of the mean

From the data set that was corrected for normality, the mean and standard deviation were used to remove bursts beyond 2 standard deviations from the mean[97]. Only ~95% of the normally distributed data was brought forth to kinetic fitting.

3.7.6 Kinetic fitting in MIL

A kinetic scheme was fitted to each global dataset using a maximum likelihood method within MIL software[98]. MIL performed dead time corrections to 18.833μs, and provides a kinetic rate constant for each component in the kinetic scheme, with an estimated standard error obtained based on the likelihood curvature at the fits maximum[61,98].

CHAPTER 4.0: RESULTS

4.1 Kinetic analysis of $\beta_{Anc}81$ containing receptors

Previously, our group showed that an ancestral β-subunit ($\beta_{Anc}81$) can act as a surrogate for the human AChR β-subunit forming hybrid ancestral-human receptors [87]. These hybrid $\beta_{Anc}81$ containing AChRs were functional, but displayed a reduced agonist sensitivity, a different unitary conductance, as well as an altered single-channel kinetic profile. The mechanistic origins of the qualitatively different kinetic profile were unclear and not examined in the initial report[87]. The first objective of my thesis was to quantitatively characterize the mechanistic difference between wild-type human, and $\beta_{Anc}81$-containing, AChRs.

In the presence of agonist, single-channel activity in cell-attached patches containing human muscle-type AChRs manifests as bursts of closely spaced openings and closings (Figure 2). The long-closed periods between bursts represent long-lived desensitized states, while activity within bursts portrays state transitions within an activation scheme (Scheme I). Single-channel activity recorded in the presence of increasing concentrations of agonist leads to bursts where the channel spends more and more time in an open state (Figure 2). This is formally represented as a burst pOpen (i.e. the probability that the channel is open within a burst). Plotting burst pOpen as a function of increasing acetylcholine concentration leads to dose response plot that is similar to the dose response relationship derived from previous whole cell macroscopic measurements (Figure 3C and Figure 3D). In both cases, $\beta_{Anc}81$-containing AChRs show a reduced sensitivity to acetylcholine, in that the maximal response elicited by ACh is reduced, as well as the EC50 for the dose response[87].

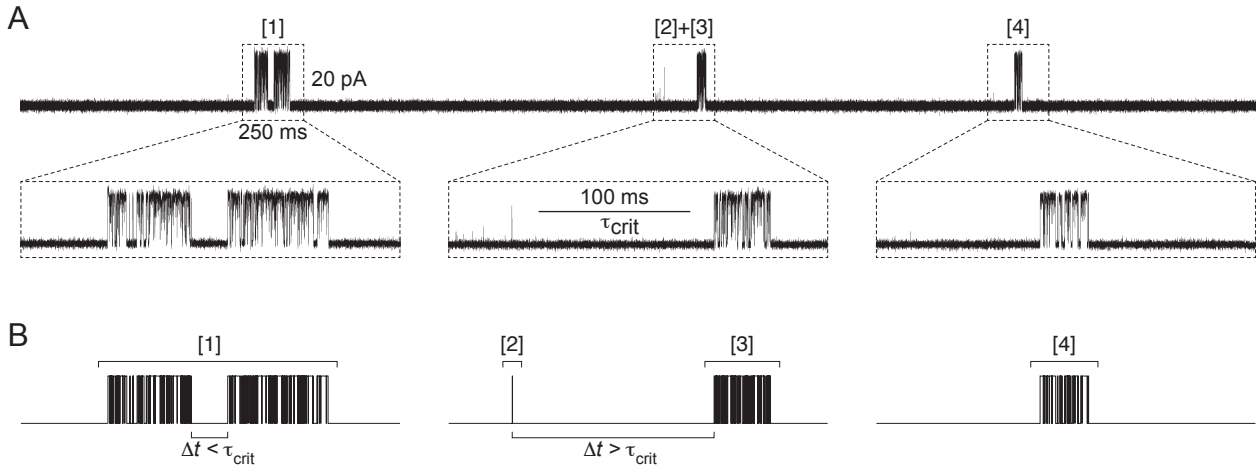

Figure 2: Single-channel burst distinction
(A) Single-channel activity of human adult muscle type acetylcholine receptor. Acetylcholine elicited single-channel recordings obtained at -120mV, at 30μM ACh, where openings are upward deflections. Data was recorded at 100kHz, and subsequently digitally filtered with a Gaussian filter to a bandwidth of 10kHz. The recording contained multiple bursts of single-channel activity, numbered [1], [2], [3], and [4]. The boxes, displaying the individual bursts, themselves represent scales bars indicating 20pA and 250ms respectively. A critical closed time(τ_{crit}), used to define a burst as shown. (B) Digitally idealized opening and closing events from the above single-channel activity. Selected closings are displayed within [1] and between [2] – [3] are highlighted.

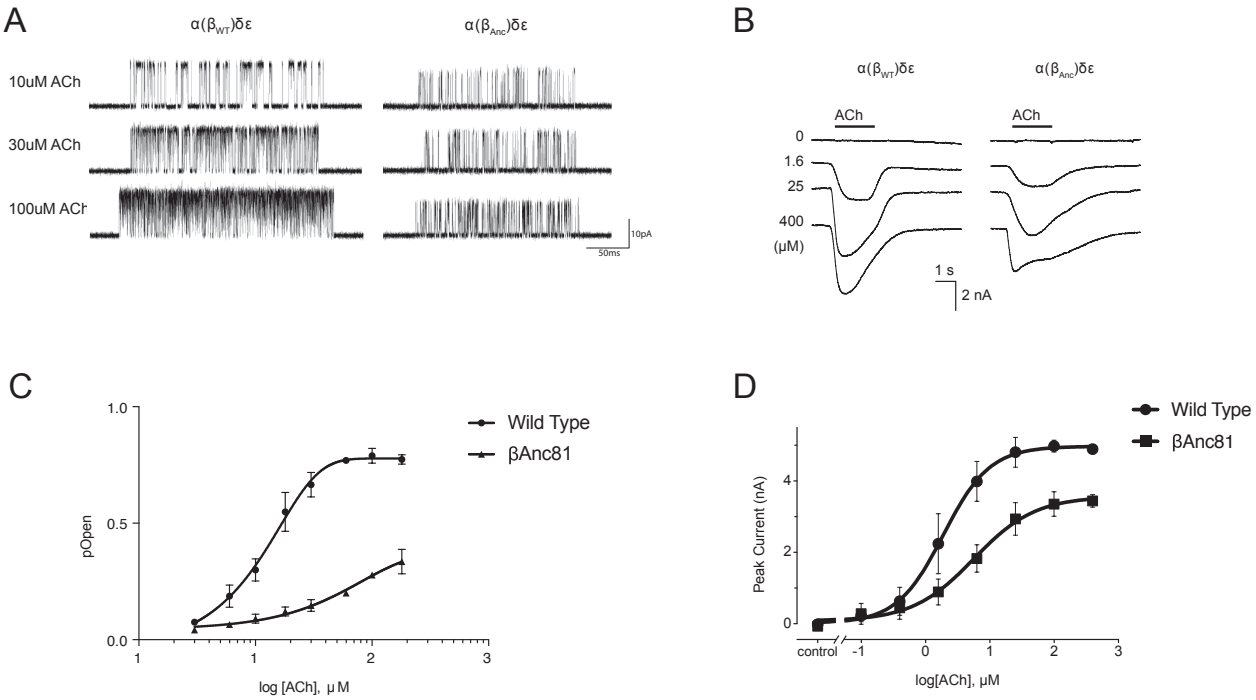

Figure 3: Microscopic and macroscopic activity changes of $\beta_{Anc}81$ containing AChRs
(A) Single-channel activity of wild type (β_{WT}) and $\beta_{Anc}81$combined with *Homo sapiens*, α, ϵ and δ wild type subunits. Acetylcholine elicited single-channel recordings obtained at -120mV, at 10μM, 30μM and 100μM, where openings are upward deflections. Data was recorded at 100kHz, and subsequently digitally filtered with a Gaussian filter to a bandwidth of 10kHz. (B) Macroscopic whole cell currents of β_{WT} and $\beta_{Anc}81$ receptors combined with complementary *Homo sapiens* subunits (α, ε, and δ). Acetylcholine was applied for a 2 second interval (bar above traces) for denoted concentrations. Data originally presented in Prinston et al. (2017) [87](C) Mean pOpen of receptors over recorded concentration range of acetylcholine ranging from 3uM to 180uM. Error bars representing standard deviation within the triplicate recordings analyzed for each concentration. Wild Type (•) and $\beta_{Anc}81$ containing receptors displayed on a logarithmic concentration scale. Denoted β subunit was combined with *Homo sapiens*, α, ϵ and δ wild type subunits. Data was fit with a sigmoidal dose response with variable slopes in GraphPad Prism 7.0. (D) Dose response relationships for WT AChRs (circles, n=5) and $\beta_{Anc}81$ containing AChRs (squares, n=5). Error bars indicate ± 1 standard deviation from the mean.

The shift in EC50 and reduced overall macroscopic response of β_{Anc}81-containing AChRs must originate from microscopic changes in the underlying channels[87]. To tease these differences apart, we acquired, in triplicate, single-channel recordings over a ACh concentration range encompassing the complete dose response. Qualitatively, for both WT and β_{Anc}-containing AChRs pOpen increases over the concentration range. To identify the origins of the changes in pOpen the single-channel activity was globally fit to Scheme I. Over the complete concentration range (Figure 4), the sequence of single-channel dwell durations from wild-type AChRs fit the modified del Castillo-Katz scheme well. Over an analogous acetylcholine concentration range, β_{Anc}81-containing AChR data (Figure 5), while not fitting the del Castillo and Katz scheme as well as WT could be fit with sufficient convergence to yield, rates that can inform the mechanistic changes that result from the ancestral subunit (Table 1).

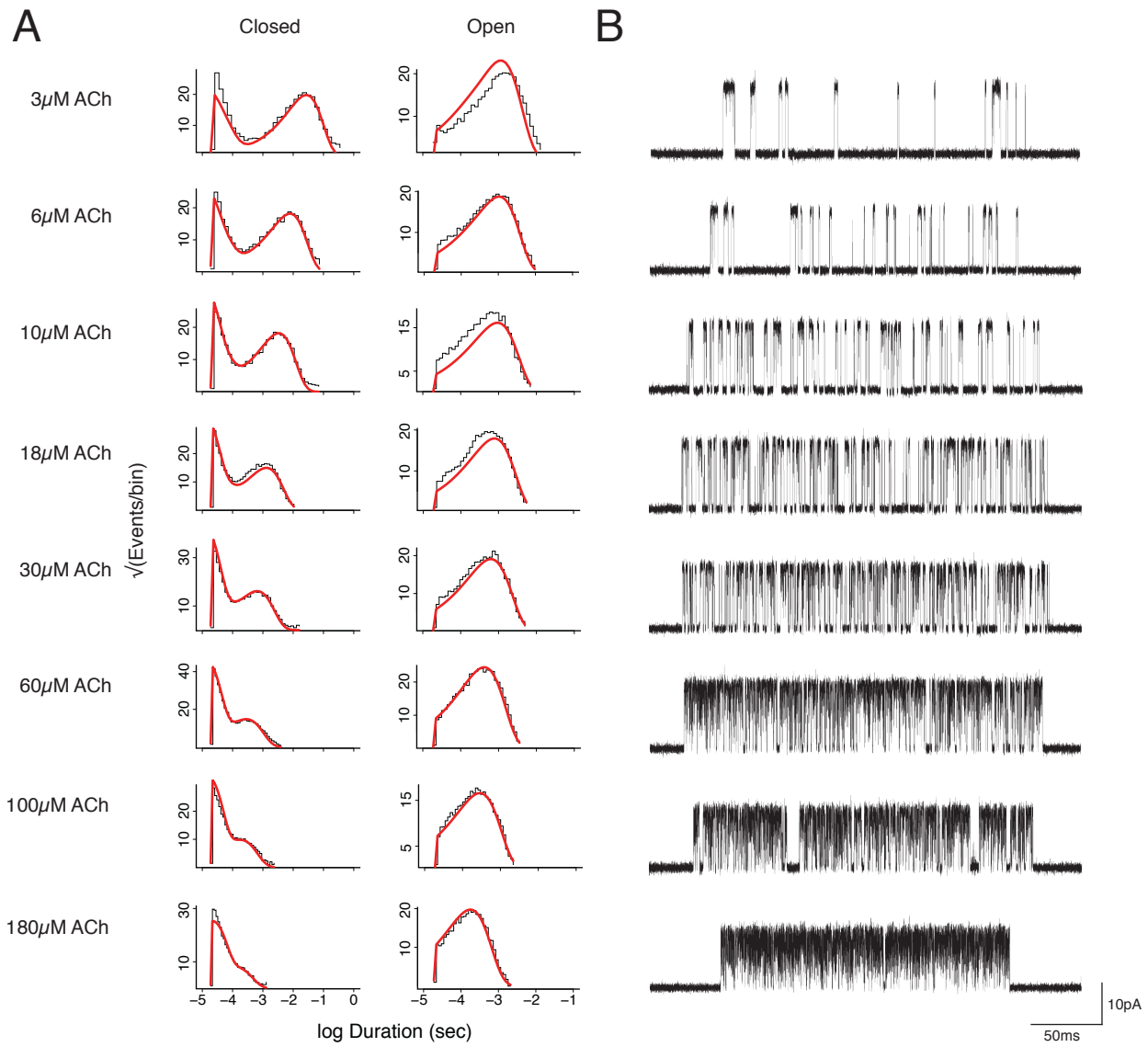

Figure 4: Single-channel analysis of wild type (WT) receptors.
(A) For each of the denoted acetylcholine (ACh) concentrations, closed and open dwell time histograms are displayed on log axis, with the global fit of the del Castillo and Katz kinetic scheme (Scheme I) overlaid. Rate constants for global fits are displayed in Table 1. (B) Wild type β subunit was combined with *Homo sapiens*, α, ϵ and δ wild type subunits. Acetylcholine elicited single-channel recordings obtained as described in Materials and Methods 3.5-3.6

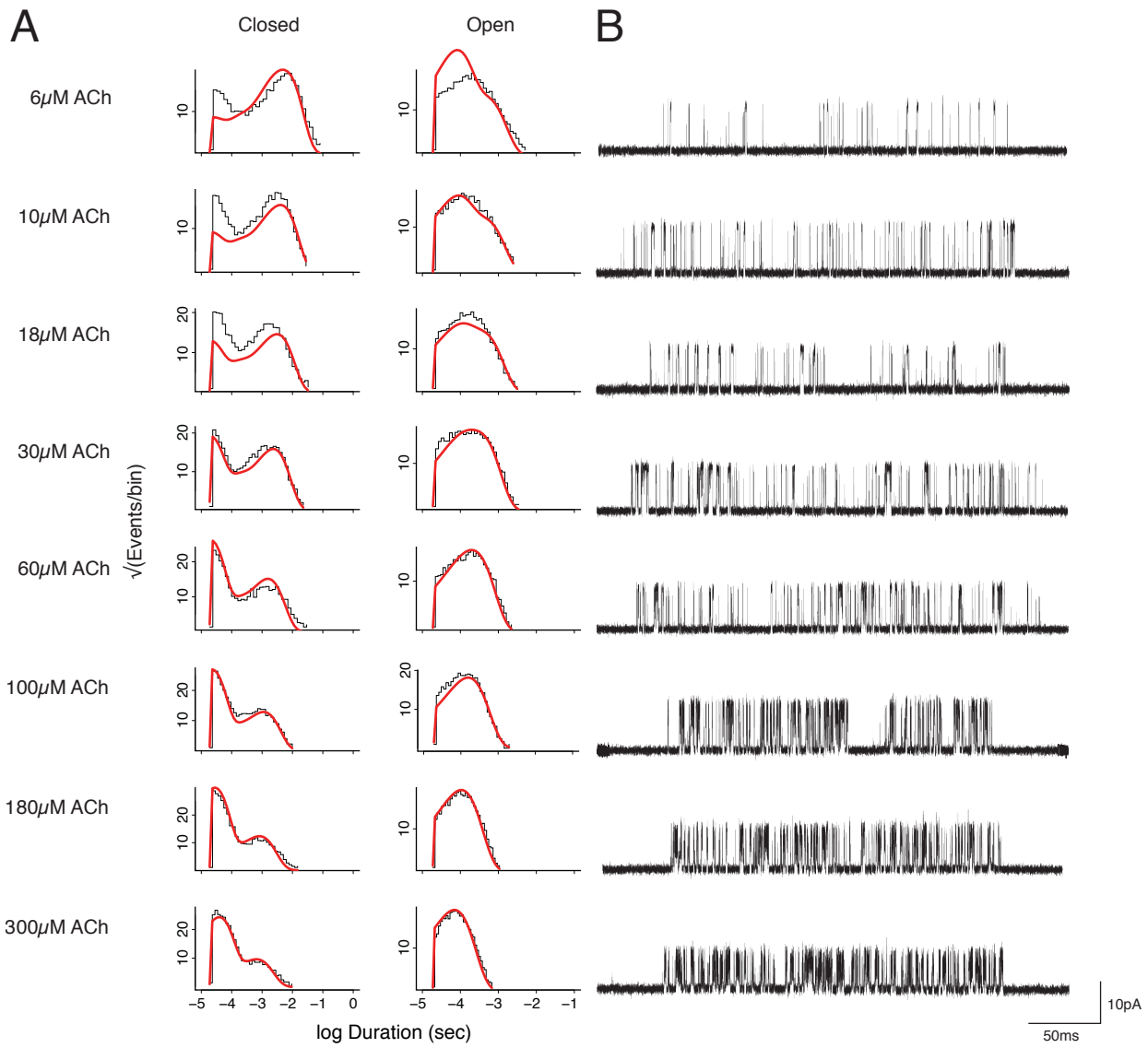

Figure 5: Single-channel analysis of $\beta_{Anc}81$ containing receptors.
(A) For each of the denoted acetylcholine (ACh) concentrations, closed and open dwell time histograms are displayed on log axis, with the global fit of the del Castillo and Katz kinetic scheme (Scheme I) overlaid. Rate constants for global fits are displayed in Table 1. (B) Ancestral $\beta_{Anc}81$ subunit was combined with *Homo sapiens*, α, ϵ and δ wild type subunits. Acetylcholine elicited single-channel recordings obtained as described in Materials and Methods 3.5-3.6

Introducing the 132 amino acid mutations (125 substitutions & 7 insertions/deletions), dispersed throughout the $\beta_{Anc}81$ subunit results in a widespread change in kinetics. Despite not being structurally involved in the agonist binding sites, the presence of the ancestral β subunit decreases all forward and reverse binding rates (Table 1). In the presence of the $\beta_{Anc}81$ subunit, singly-liganded openings become more favorable, with a decrease in double liganded openings, as a result. The first binding equilibrium rate decreased, favouring the forward binding, whereas the second binding equilibrium increased, favouring agonist dissociation. The same trend is present within the gating equilibrium rates, where the first gating equilibrium rate is increased, while the doubly liganded gating equilibrium is reduced. These changes in gating equilibriums can be attributed to the changes of the forward gating rates (β), while the channel closing remain consistent. Blocking rates remain consistent, supporting the pore architecture results in block to the same degree.

4.2 Relationships in evolutionary generated β sequences

WT and $\beta_{Anc}81$-containing AChRs differ by 132 mutations [87]. To identify which of these mutations are responsible for the observed mechanistic differences, we returned to the original β_{Anc} phylogeny and sequence alignment. In the original tree, ancestral nodes were sequentially numbered, and βanc81 corresponds to node 81. For this reason, we refer to this ancestor as βanc81. There are several nodes of interest along the trajectory from $\beta_{Anc}81$ to WT (Figure 6). In particular, $\beta_{Anc}84$, $\beta_{Anc}85$, and $\beta_{Anc}86$ subdivide the 132 differences between $\beta_{Anc}81$ and human WT (Figure 6). We resurrected each of these ancestors along the evolutionary trajectory, and qualitatively assessed the single-channel activity of hybrid AChRs containing each of the resurrected ancestral β subunits. Implicating one or more of the residues in the interval between $\beta_{Anc}85$ and $\beta_{Anc}86$, single-channel conductance regains wild-type phenotype over this period (Figure 7). In contrast, single-channel pOpen changes between $\beta_{Anc}81$ and $\beta_{Anc}84$, indicating residues within this evolutionary interval are largely responsible for the kinetic differences between $\beta_{Anc}81$ and WT.

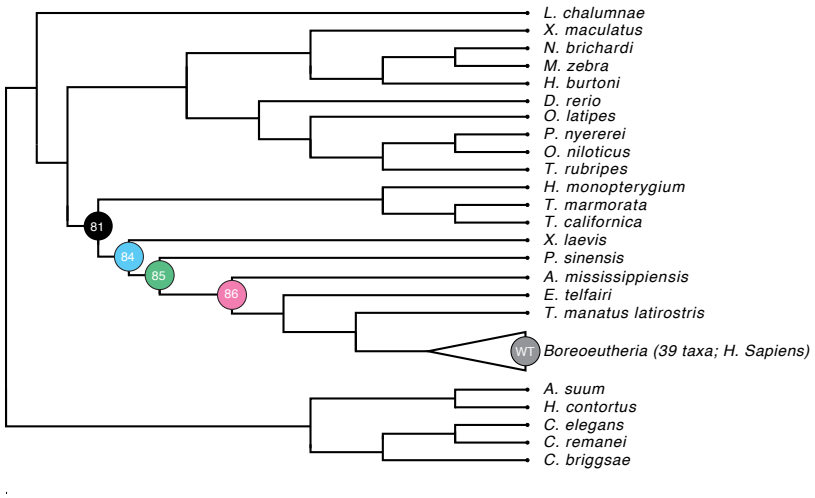

Figure 6: Maximum likelihood phylogeny of the muscle type AChR β subunit guided by amino acid sequences.

Nodes investigated in this study are highlighted. The human wild-type subunit, highlighted in grey, is present within *Boreoeutheria*. $\beta_{Anc}81$ (black) the last common ancestor shared between *Torpedo marmorata* and *Homo sapiens*. Other important nodes; $\beta_{Anc}84$ (blue), $\beta_{Anc}85$ (green) and $\beta_{Anc}85$ (pink) are also highlighted. For the detailed phylogenetic tree, see Prinston et.al. [87]

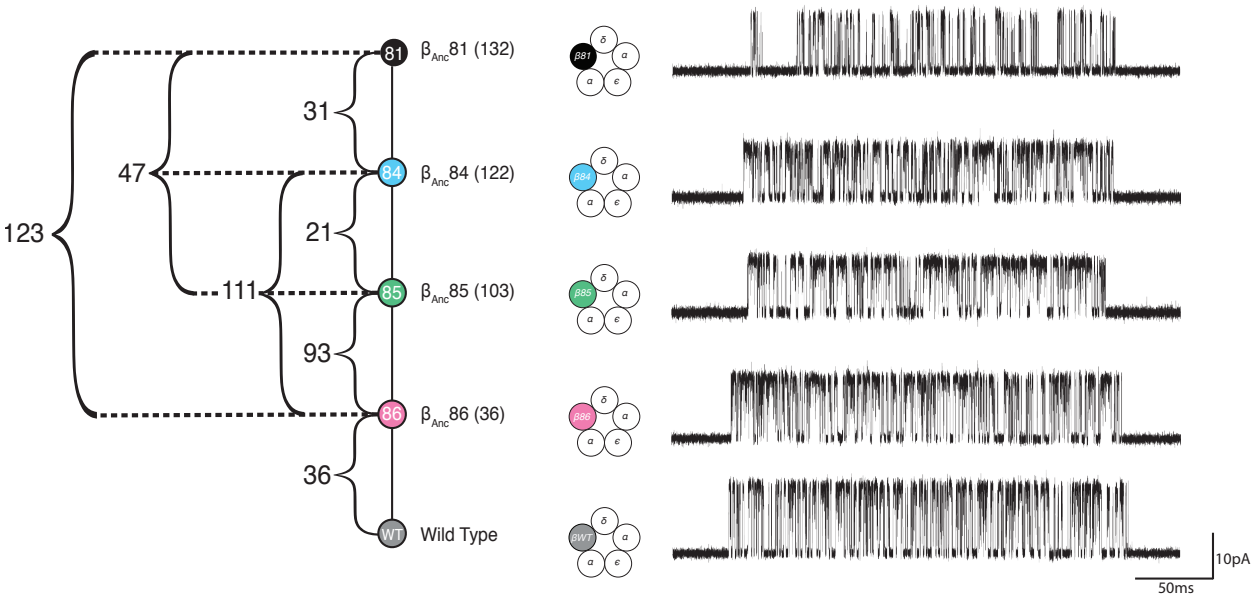

Figure 7: Amino acid substitution change along evolutionary tree and associated single-channel activity.

Amino acid substitutions between evolutionary time points as displayed. Amino acid substitutions from wild type *Homo sapiens* β subunit sequence denoted in brackets. Mutant/Ancestral β subunits were combined with *Homo sapiens*, α, ϵ and δ wild type subunits. Single-channel recordings were elicited in the presence of 30μM Acetylcholine. Recordings obtained as described in Materials and Methods 3.5-3.6

$\beta_{Anc}84$ is the following ancestor along the evolutionary trajectory after $\beta_{Anc}81$, which differs by 31 amino acids (31 substitutions) from $\beta_{Anc}81$, and 122 (7 insertions/deletions & 115 substitutions) residues from WT. Both the open and closed dwell time histograms could be fit to the del Castillo and Katz kinetic scheme over the entire concentration range. Heteropentamers containing the $\beta_{Anc}84$ subunit regain WT pOpens (Figure 8), implicating residues within this evolutionary timeframe. To confirm $\beta_{Anc}84$ exhibits wild-type like kinetic behavior, a full dose response was performed (Figure 9). Both the binding and apparent gating rates of heteropentamers containing the $\beta_{Anc}84$ subunit, are shifted to be more wild-type like (Table 1)

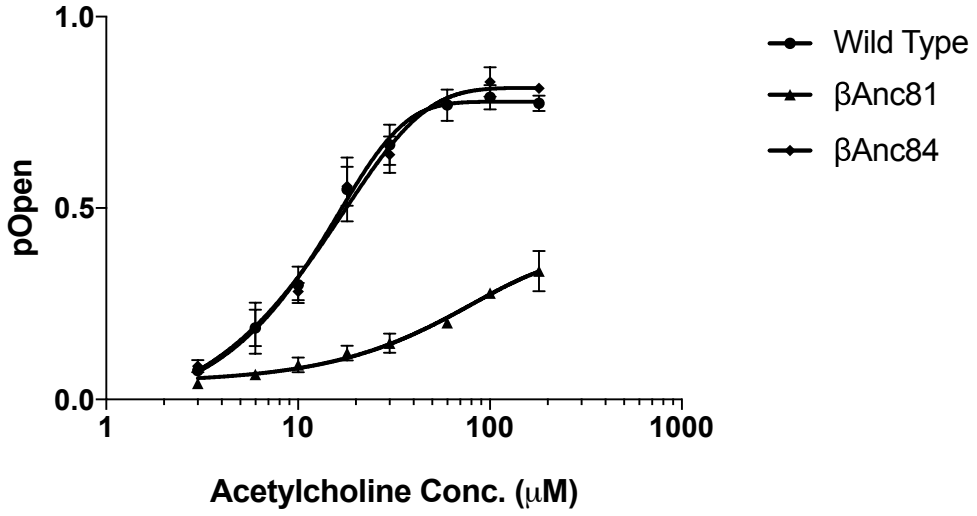

Figure 8:Open probabilities as a function of acetylcholine concentration
Mean pOpen of receptors over the recorded concentration range of acetylcholine ranging from 3uM to 180uM. Error bars representing standard deviation within the triplicate recordings analyzed for each concentration. Wild type and receptors containing denoted ancestral β subunit with complementary wild type subunits displayed on logarithmic scale. Data was fit with a sigmoidal dose response with variable slopes in GraphPad Prism 7.0.

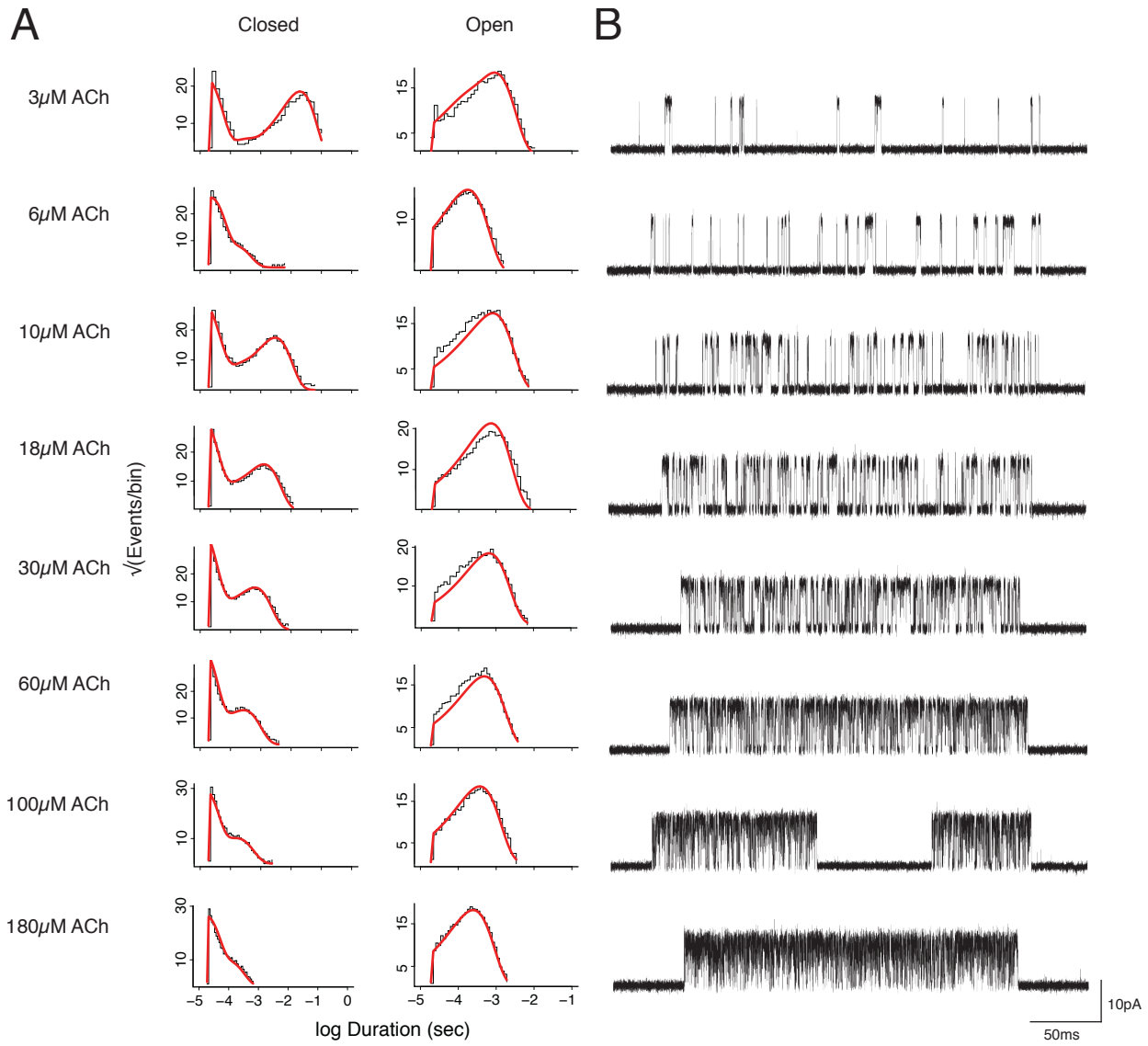

Figure 9: Single-channel analysis of $\beta_{Anc}84$ containing receptors.
(A) For each of the denoted acetylcholine (ACh) concentrations, closed and open dwell time histograms are displayed on a log axis, with the global fit of the del Castillo and Katz kinetic scheme (Scheme I) overlaid. Rate constants for global fit data are displayed in Table 1. (B) Ancestral $\beta_{Anc}84$ subunit was combined with *Homo sapiens*, α, ϵ and δ wild type subunits. Acetylcholine elicited single-channel recordings obtained as described in Materials and Methods 3.5-3.6

4.3 Pore mutations of $\beta_{Anc}81$

Having confirmed that $\beta_{Anc}84$ exhibits kinetics closer to WT, we wanted to determine which residues were responsible for regaining the WT-like phenotype. $\beta_{Anc}81$ and $\beta_{Anc}84$ differ by 31 amino acids. The questions is: which of these 31 residues are most responsible for the shift in phenotype? Based on observations made by J. Emlaw, an MSc student in the lab studying the origins of the differences in conductance between βanc81-containing and WT channels, we focused on the pore-lining second transmembrane segment (M2) of the AChR pore (Figure 10). This privileged region of the pore is a well-known determinant of both single-channel conductance and gating kinetics[49,51,99].

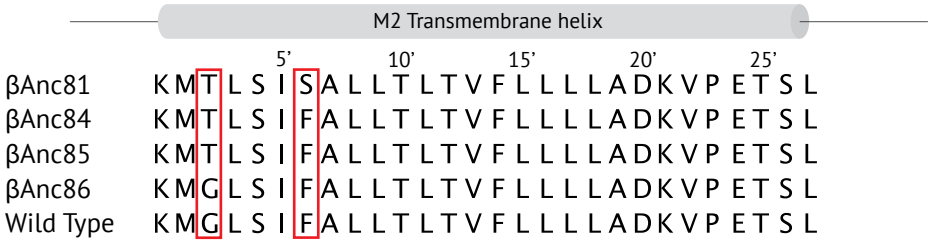

Figure 10: β-subunit M2 transmembrane helices.
M2 helix domain along the evolutionary tree. The pore lining helix residues are denoted as prime numbers increasing from N-terminus to C-terminus. Residues highlighted denotes residues that have changes along the evolutionary path between $\beta_{Anc}81$ to the *Homo sapiens* wild type sequence.

Residues within the M2 α-helix are numbered 0' ("zero prime") to 25', in the N- to C-terminal direction (Figure 10). Of note, the 2' residue, a known determinant of conductance[48,55,57,100,101], is a threonine in $\beta_{Anc}81$ and mutates to a glycine between $\beta_{Anc}85$ and $\beta_{Anc}86$, coinciding with the main increase in single-channel conductance along the trajectory to WT. Substitutions of a glycine to threonine resulted in a 20% decrease in single-channel conductance. [48,55,57,100,101] Consistent with these previous findings, unpublished observations by J. Emlaw, and confirmed here, show that when the threonine residue in βanc81 is substituted for the WT glycine, WT single-channel conductance is restored (Figure 7). The only other difference between βanc81 and WT in the M2 region is the residue in the 6' position, which is a serine in $\beta_{Anc}81$, and a phenylalanine in WT. Interestingly, substitution of phenylalanine for the serine in βanc81 happens in the evolutionary gap between $\beta_{Anc}81$ and $\beta_{Anc}84$ coinciding with the qualitative change in single-channel kinetics towards WT (Figure 7).

4.4 $\beta_{Anc}81$ pore mutant kinetic analysis

Based on the hypothesis that the 6' residue was responsible for the change in single-channel kinetics, we substituted the 6' serine in $\beta_{anc}81$ to the 6' phenylalanine present in both WT and $\beta_{Anc}84$, and collected a single-channel data set encompassing the full acetylcholine concentration range. The $\beta_{Anc}81$ S6'F substitution to phenylalanine leads to an increase in burst pOpen over the entire ACh concentration range (Figure 11). This increase in pOpen, which is large enough to be discerned by the eye, does not reach that observed in the WT AChRs. Kinetic fitting shows that the presence of the 6' phenylalanine, both the mono-liganded and di-liganded binding and unbinding rates are slower (Figure 12). Consistent with what was observed in $\beta_{Anc}81$ containing receptors, apparent gating of doubly liganded AChRs is favored over mono-liganded openings (Θ_2 greater than Θ_1). The di-liganded opening rate (β_2) is faster than that observed in the $\beta_{Anc}81$, which leads to increased openings, and higher saturation of channel open times. Although the kinetics are not identical to wild type, the S6'F substitution in $\beta_{Anc}81$ leads to a notable shift in kinetics towards that observed in wild type receptors (Table 1 & Figure 14).

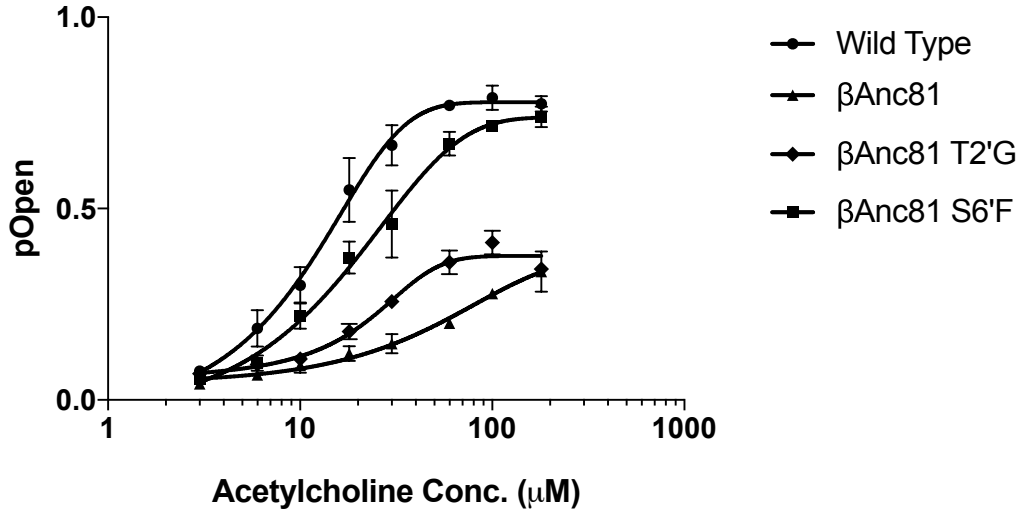

Figure 11: Open probabilities as a function of acetylcholine concentration
Mean pOpen of receptors over recorded concentration range of acetylcholine ranging from 3uM to 180uM. Error bars representing standard deviation within the triplicate recordings analyzed for each concentration. Wild type and receptors containing denoted ancestral β subunit with complementary wild type subunits, displayed on both regular and logarithmic scales. Data was fit with a sigmoidal dose response with variable slopes in GraphPad Prism 7.0.

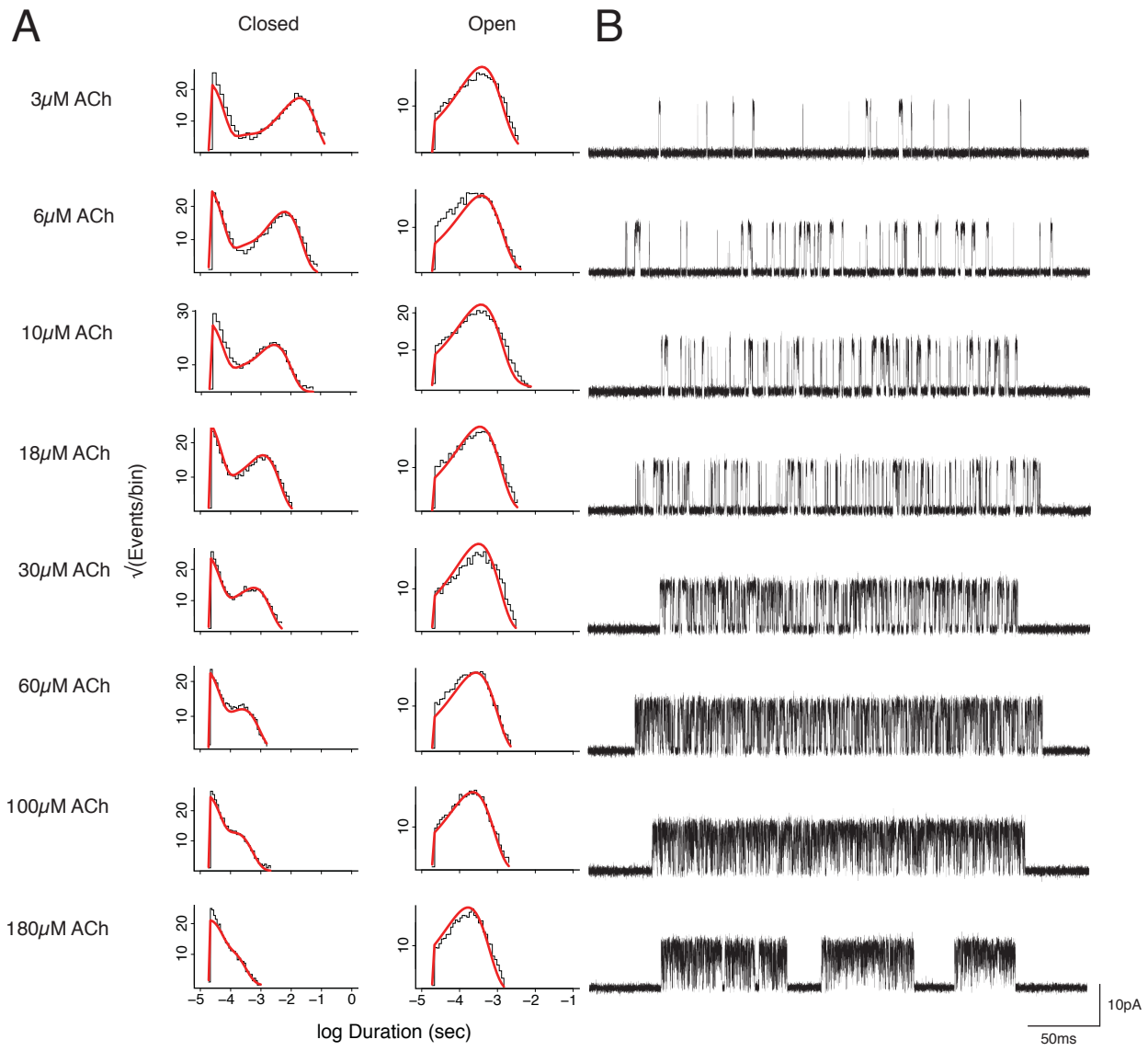

Figure 12: Single-channel analysis of βAnc81 S6'F receptors.

(A) For each of the denoted acetylcholine (ACh) concentrations, closed and open dwell time histograms are displayed on a log axis, with the global fit of the del Castillo and Katz kinetic scheme (Scheme I) overlaid. Rate constants for global fit data are displayed in Table 1. (B) Ancestral $\beta_{Anc}81$ S6'F subunit was combined with *Homo sapiens*, α, ϵ and δ wild type subunits. Acetylcholine elicited single-channel recordings obtained as described in Materials and Methods 3.5-3.6

To examine the contribution of the 2' residue to kinetics, we also installed a T2'G substitution, and collected a complete single-channel data set encompassing the full ACh concentration range. In the $\beta_{Anc}81$ background, despite the T2'G substitution leading to a marked increase in single-channel amplitude (and thus conductance), from a kinetics standpoint the substitutions leads to a marginal increase in burst pOpen (Figure 11). Kinetic fits confirm that the T2'G $\beta_{Anc}81$ mutant exhibits similar kinetics to those of $\beta_{Anc}81$(Figure 13) (Table 1 & Figure 14).

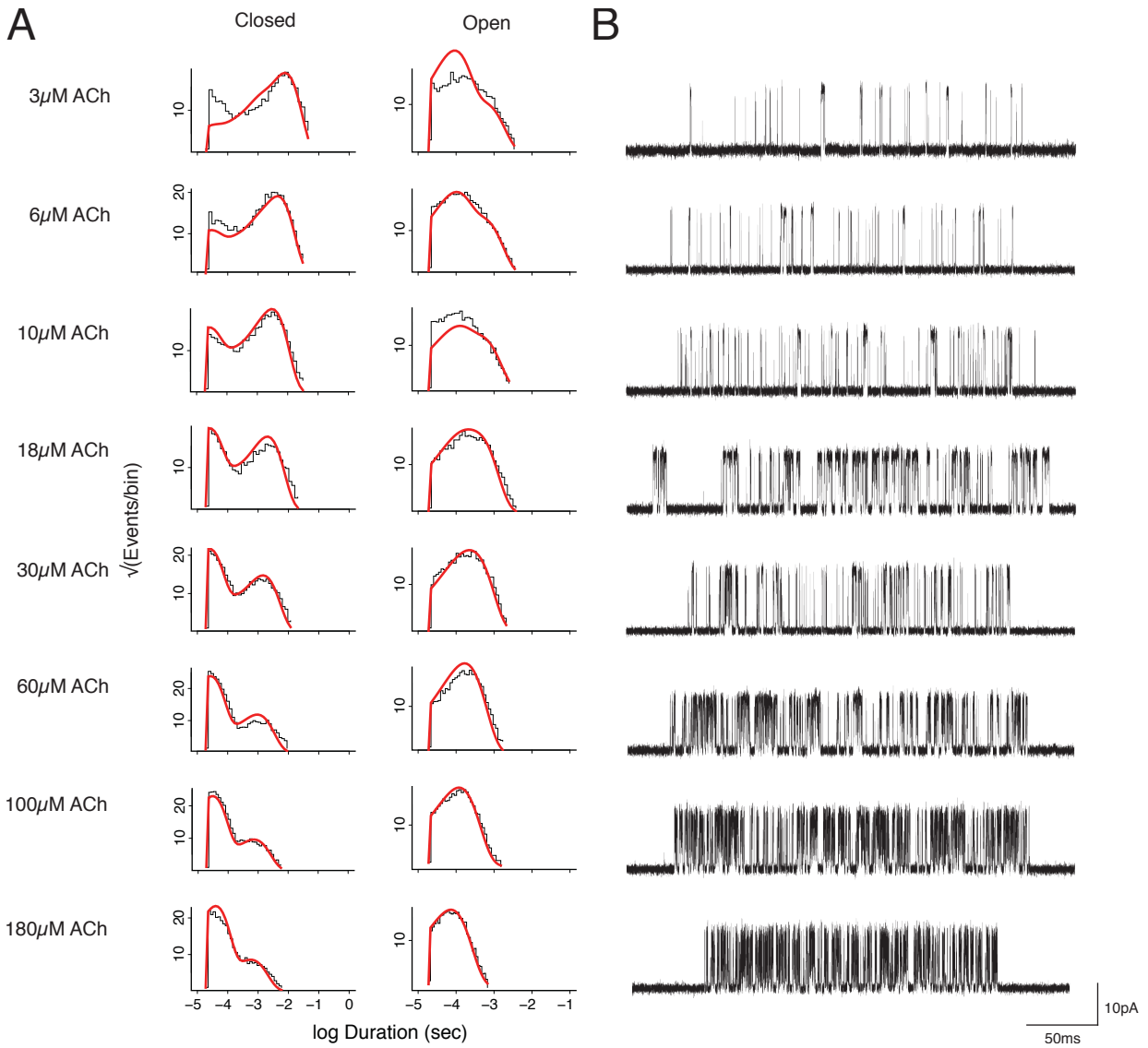

Figure 13: Single-channel analysis of βAnc81 T2'G receptors.

(A) For each of the denoted acetylcholine (ACh) concentrations, closed and open dwell time histograms are displayed on a log axis, with the global fit of the del Castillo and Katz kinetic scheme (Scheme I) overlaid. Rate constants for global fit data are displayed in Table 1. (B) Ancestral $\beta_{Anc}81$ T2'G subunit was combined with *Homo sapiens*, α, ϵ and δ wild type subunits. Acetylcholine elicited single-channel recordings obtained as described in Materials and Methods 3.5-3.6

Table 1: Kinetics of muscle type AChR-activation by acetylcholine.
Single-channel kinetic rates of wild type receptors, and receptors containing denoted ancestral β subunit with complementary wild type subunits. Binding and gating rates and errors were computed by MIL software. The channel gating equilibrium constants $\Theta=\beta_n/\alpha_n$ and the dissociation constant $K = k_{-1}/k_{+1}$. All calculated rates are rounded, with exact rate values provided in supplemental Table 1. Example of error propagation calculation or equilibrium constants provided in supplemental information.

Binding	Wild Type	βAnc84	βAnc81 S6'F	βAnc81 T2'G	βAnc81
k+1	650 ± 34	317 ± 9	304 ± 6	189 ± 5	72 ± 2
k-1	14400 ± 1000	4100 ± 140	3500 ± 110	660 ± 50	140 ± 10
K1 (μM)	22 ± 1.9	13 ± 0.6	12 ± 0.4	3 ± 0.3	2 ± 0.2
k+2	325 ± 20	160 ± 5	150 ± 3	100 ± 2	36 ± 1
k-2	26500 ± 400	27000 ± 240	24000 ± 170	8500 ± 220	6500 ± 200
K2 (μM)	81 ± 5	172 ± 5	158 ± 3	90 ± 3	179 ± 6
k+b	215 ± 3	175 ± 4	160 ± 5	190 ± 2	160 ± 2
k-b	106500 ± 800	120000 ± 1200	108000 ± 1500	52000 ± 450	70000 ± 700
Kb (μM)	500 ± 8	700 ± 17	690 ± 22	280 ± 3	450 ± 7

Gating	Wild Type	βAnc84	βAnc81 S6'F	βAnc81 T2'G	βAnc81
β1	33 ± 2	77 ± 3	32 ± 3	400 ± 10	300 ± 4
α1	8800 ± 650	10400 ± 400	1300 ± 35	13000 ± 450	15000 ± 400
Θ1	0.004 ± 0.0004	0.007 ± 0.0004	0.025 ± 0.002	0.03 ± 0.001	0.02 ± 0.0006
β2	14000 ± 450	35000 ± 700	42000 ± 625	2950 ± 95	2900 ± 90
α2	1100 ± 10	1900 ± 22	5100 ± 57	2000 ± 20	2300 ± 20
Θ2	13 ± 0.4	18 ± 0.4	8 ± 0.2	1.5 ± 0.1	1.3 ± 0.04

Rate constants were estimated from kinetic fitting of del Castillo and Katz scheme (Scheme I) to a global data set over a range of acetylcholine ACh concentrations. Errors were computed by MIL software. The channel gating equilibrium constants $\Theta=\beta_n/\alpha_n$ and the dissociation constant $K = k_{-1}/k_{+1}$.

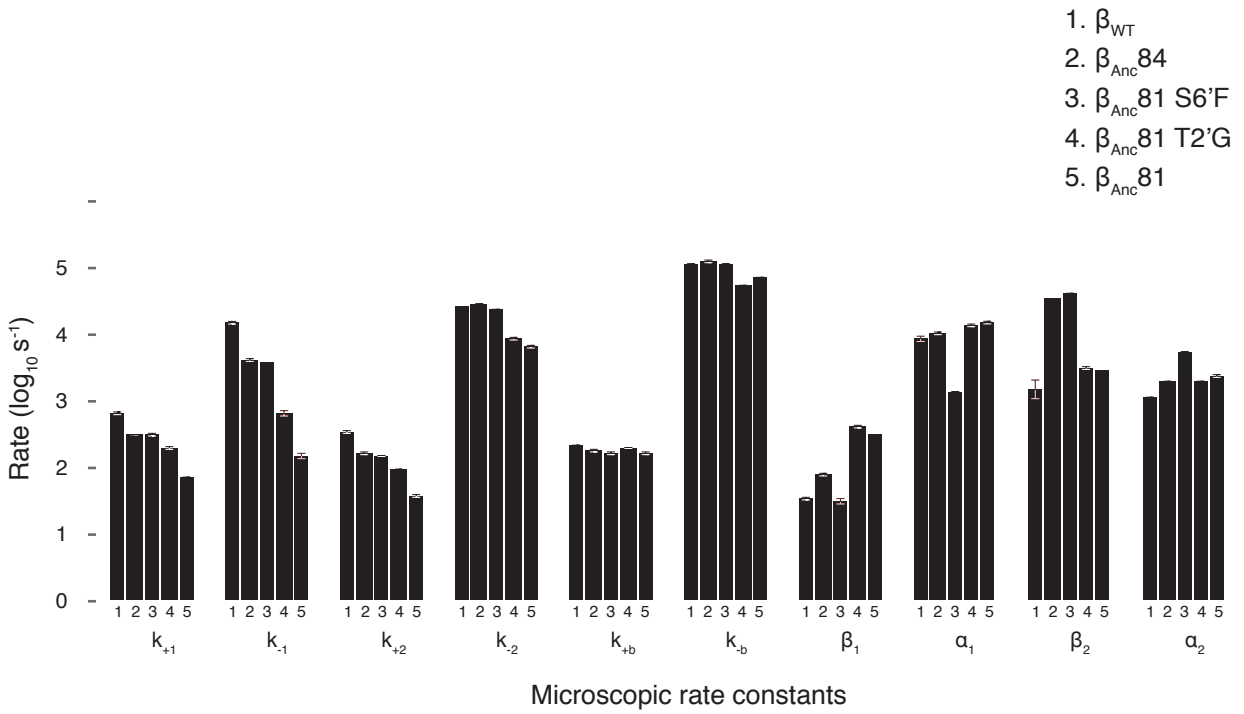

Figure 14: Microscopic rate constants of muscle-type AChR-activated by acetylcholine
Single-channel kinetic rates of wild type receptors, and receptors containing denoted ancestral β subunit with complementary wild type subunits. Microscopic rate constants, provided in Table 1 were computed by MIL software. Denoted error bars refer to computed rate constant standard deviations from MIL software.

To further validate the influence of the 6’ residue on AChR kinetics, we reverse evolved the WT human β subunit by substituting a 6' serine for the phenylalanine present in WT. Qualitatively, burst pOpen decreases as hypothesized (Figure 15).

Figure 15: Verification of the 6' residues effect on kinetics.
Indicated β subunit was combined with *Homo sapiens*, α, ϵ and δ wild type subunits. 30μM Acetylcholine elicited single-channel recordings obtained at -120mV, where openings are upward deflections. Single-channel recordings obtained as described in Materials and Methods 3.5-3.6

CHAPTER 5.0: DISCUSSION OF RESULTS

Using single-channel analysis we have quantified the kinetic differences between β_{Anc}-containing and WT AChRs. Contrary to what might be expected for a subunit that does not participate directly in agonist binding, kinetic fits show that replacement of the human WT β-subunit with β_{Anc} results in changes in both the kinetics of channel gating and agonist binding. Taking advantage of our mapped evolutionary trajectory (Figure 6), we narrowed in on which of the 132 mutations between β_{Anc} and the human WT subunit are responsible for these kinetic differences. Our analysis led us to the interval between β_{Anc}81 and β_{Anc}84, which only differs by 31 residues. Of these we focused in on the 6' position of the M2 pore-lining helix and substituted a phenylalanine present in β_{Anc}84 into β_{Anc}81. This single point mutation caused the β_{Anc}81-containing kinetics to be more WT-like. Consistent with the hypothesis that this residue contributes to AChR single-channel kinetics, reverse evolving the 6' position of the human WT subunit, by substituting serine for the WT phenylalanine qualitatively shifts the kinetic behavior to resemble β_{Anc}81-containing AChRs. The finding of the β6' position contributes to AChR single-channel kinetics is novel and has not been shown previously.

The only other residue in M2 to change between β_{Anc}81 and WT is in the 2' position, a full helical turn from 6'. In β_{Anc}, this residue is a threonine, while in WT it is a glycine. Substitution of a glycine into β_{Anc} fails to shift the single-channel kinetics towards WT, despite having a marked effect on single-channel conductance. It is surprising that these two residues, which are in close proximity to one another, in a privileged location of the pore, appear to have divergent contributions to single-channel kinetics. To demonstrate independent contributions to kinetics, our lab has begun mutant-cycle analysis (i.e. comparison with the 2' and 6' double mutants).

To facilitate comparisons, all mutants were kinetically characterized within the framework of the modified del Castillo- Katz scheme (Scheme I), which included a di-liganded open-channel agonist blocked state. Wild type, β_{Anc}84-containing, and β_{Anc}81S6'F-containing heteropentamers were all well fit by this mechanistic scheme, as kinetic fits superimposed well over dwell time histograms encompassing the entire agonist concentration range (Figures 4, 9 and 12). In contrast, dwell time histograms for both β_{Anc}81-containing, and β_{Anc}81T2'G-containing heteropentamers did not superimpose nearly as well, especially at lower agonist concentrations (see Figure 5 and 13), where fits overestimated the incidence of short-lived openings and underestimated the prevalence of short-lived closings. This discrepancy hints that a more complicated kinetic model, including intermediate closed states [72,89], may be necessary to adequately describe the single-channel data for these mutants. Determining which model best describes the data is a priority for future work.

Previous whole-cell data has shown reduced apparent cooperativity of agonist-induced macroscopic currents for β_{Anc}-containing AChRs [87]. In principle, this reduction in apparent cooperativity could have arisen from changes in agonist binding and/or channel gating. Our kinetic fits corroborate the apparent negative cooperativity, and show that it results from a ~20-fold reduction in the relative affinity of the first and second binding steps (i.e. K_{D1}/K_{D2} for β_{Anc} vs. WT), as well as the ~100-fold reduction in the relative efficiency of di- vs. mono-liganded gating (i.e. $\Theta 2/\Theta 1$ for β_{Anc} vs. WT) (see Table 1)

Using the evolutionary biochemistry approach to investigate structure-function relationships in the AChR, we uncovered the importance of the 6' residue on AChR single-channel kinetics. Previously reported by Charnet et al (1990), and in Hilf et al (2010), the 6' residue was found important for ion channel block [68,102]. Aside from ion channel block, our findings are

the first to note the 6' residues importance on the kinetics of the adult muscle type AChR. In the late 1990's, researchers discovered the importance of 9' residues importance in regulating ion channel kinetics[51]. Mutating the 9' residue increases spontaneous opening, destabilizing the closed conformation of the ion channel. It is appropriate that the 6' residues, one helical turn away, impacts the kinetics of the ion channel, and rescues wild-type like function[103] (Figure 16). Despite successfully rescuing wild-type kinetics, other residues within the β1 structure are influencing both the binding and apparent gating kinetics of the receptor. To fully understand which other residues are influencing the kinetics of the receptor, along with the 6' site, additional studies must be performed.

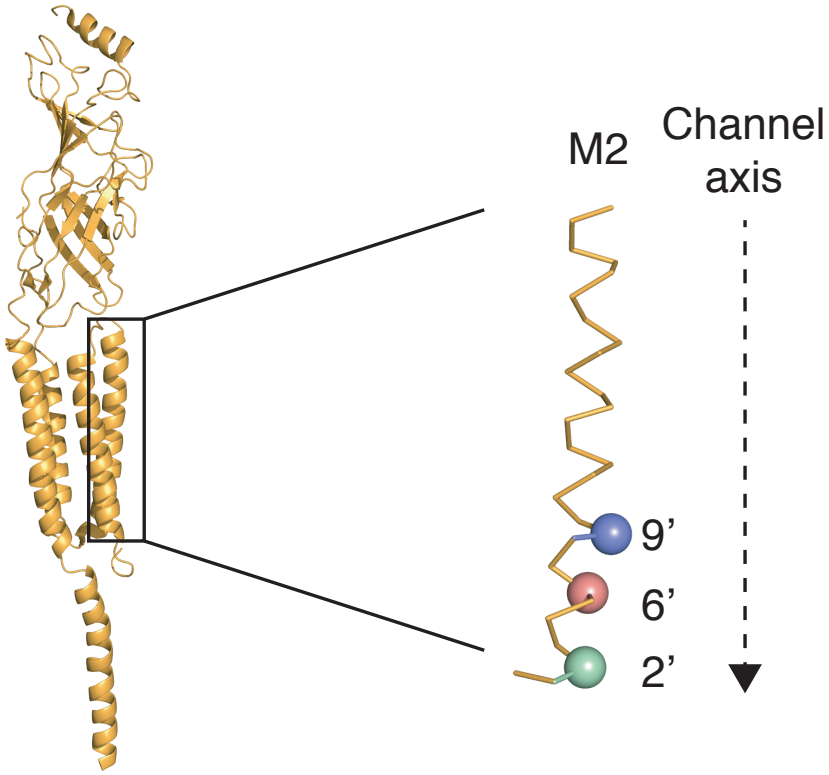

Figure 16: Location of the M2 2’ and 6’ residues along the channel axis
Acetylcholine receptor subunit structure with the pore lining transmembrane helix (TM2) highlighted. Ribbon diagram (right) depicts important residues from one subunit that lines the ion conducting pore/channel axis. Highlighted residues include; 9’, which has been previously proved to influence channel kinetics, and the 6’ and 2’ residues, discussed throughout which play a role in the functional changes of the receptor, on both the kinetics and conductance, respectively.

Further investigation into a higher order mechanistic scheme is required to elucidate the origins of the overestimation of short-lived openings and underestimation of short-lived closing. The current phylogeny used to generate $\beta_{Anc}81$ (84, 85 and 86) was generated entirely based on protein sequence, a molecular phylogeny. As published in Tessier et. al (2017), a species phylogeny differs from the molecular phylogeny but, ensures that the included sequences are of high quality and follow the accepted tree of life[104]. For this reason, our lab is generating new phylogenies to reconstruct more representative ancestors of the 4 subunits (α1, β1, δ, ε/γ). Once complete, the activity of ancestral heteropentamers will be quantified, and will provide insight into other functional residues within the 4 subunits of the receptor that contribute to their ability to cooperate with one another.

CHAPTER 6.0: CONCLUSIONS

In conclusion, the ancestral reconstruction led to the identification of two residues that are responsible for a significant amount of the functional changes. The 6' residue, which evolved along the evolutionary trajectory had a greater impact on the kinetics of the ion channel, compared to the 2' position which primarily influences channel conductance. Using an ancestral reconstruction has thus proven useful for the identification of residues that are functionally important. The 6' residue was shown to be important in channel kinetics, restoring wild-type like kinetics within the $\beta_{Anc}81$ background.

SECTION 7.0: REFERENCES

1 Sine, S. M. (2012) End-plate acetylcholine receptor: structure, mechanism, pharmacology, and disease. Physiological Reviews, American Physiological Society **92**, 1189–1234.

2 Raftery, M. A., Hunkapiller, M. W., Strader, C. D. and Hood, L. E. (2018) Acetylcholine Receptor: Complex of Homologous Subunits. Science 1454–1459.

3 Guda, P., Bourne, P. E. and Guda, C. (2007) Conserved motifs in voltage-sensing and pore-forming modules of voltage-gated ion channel proteins. Biochemical and Biophysical Research Communications **352**, 292–298.

4 Biggin, P. C. and Sansom, M. S. P. (2003) Mechanosensitive Channels: Stress Relief. Current Biology **13**, 183–185.

5 Li, S.-X., Huang, S., Bren, N., Noridomi, K., Dellisanti, C. D., Sine, S. M. and Chen, L. (2011) Ligand-binding domain of an α7-nicotinic receptor chimera and its complex with agonist. Nat Neurosci **14**, 1253–1259.

6 Reyes-Parada, M., Iturriaga-Vasquez, P., Reyes-Parada, M. and Iturriaga-Vasquez, P. (2016) The development of novel polypharmacological agents targeting the multiple binding sites of nicotinic acetylcholine receptors. Expert Opinion on Drug Discovery, Taylor & Francis **11**, 969–981.

7 Albuquerque, E. X., Pereira, E. F. R., Alkondon, M. and Rogers, S. W. (2009) Mammalian Nicotinic Acetylcholine Receptors: From Structure to Function. Physiological Reviews **89**, 73–120.

8 Mukhtasimova, N., Lee, W. Y., Wang, H.-L. and Sine, S. M. (2009) Detection and trapping of intermediate states priming nicotinic receptor channel opening. Nature **459**, 451–454.

9 Goldman, D., Deneris, E., Luyten, W., Kochhar, A., Patrick, J. and Heinemann, S. (1987) Members of a Nicotinic Acetylcholine Receptor Gene Family Are Expressed in Different Regions of the Mammalian Central Nervous System. Cell Press **48**, 965–973.

10 Jaiteh, M., Taly, A. and Hénin, J. (2016) Evolution of Pentameric Ligand-Gated Ion Channels: Pro-Loop Receptors. PLoS ONE (Bertrand, S., ed.) **11**, e0151934–24.

11 Connolly, J., Deneris, E., Goldman, D., Heinemann, S., Patrick, J. and BOulter, J. (1987) Functional expression of two neuronal nicotinic acetylcholine receptorsfromcDNA clones. Proc Natl Acad Sci USA **84**, 7763–7767.

12 Ortells, M. O. and Lunt, G. G. (1995) Evolutionary history of the ligand-gated ion-channel superfamily of receptors. Elsevier **18**, 121–128.

13 Changeux, J.-P. (2012) The Nicotinic Acetylcholine Receptor: The Founding Father of the Pentameric Ligand-gated. J. Biol. Chem. **287**, 40207–40215.

14 Dani, J. A. (2001) Overview of Nicotinic Receptors and Their Roles in the Central Nervous System. Socierty of Biological Psychiatry **49**, 166–174.

15 Green, W. N. and Wanamaker, C. P. (1997) The Role of the Cystine Loop in Acetylcholine Receptor Assembly*. J. Biol. Chem. **272**, 20945–20953.

16 Nys, M., Kesters, D. and Ulens, C. (2013) Structural insights into Cys-loop receptor function and ligand recognition. Biochemical Pharmacology, Elsevier Inc. **86**, 1042–1053.

17 Thompson, A. J., Lester, H. A. and Lummis, S. C. R. (2010) The structural basis of function in Cys-loop receptors. Quarterly Reviews of Biophysics, University of Ottawa - Library Network **43**, 449–499.

18 Chua, H. C. and Chebib, M. (2017) GABAA Receptors and the Diversity in their Structure and Pharmacology. Ion Channels DownUnder 1st ed., pp 1–34, Elsevier Inc.

19 Yu, R., Hurdiss, E., Greiner, T., Lape, R., Sivilotti, L. and Biggin, P. C. (2014) Agonist and Antagonist Binding in Human Glycine Receptors. Biochemistry **53**, 6041–6051.

20 Barnes, N. M., Hales, T. G., Lummis, S. C. R. and Peters, J. A. (2009) The 5-HT3 receptor – the relationship between structure and function. Neuropharmacology, Elsevier Ltd **56**, 273–284.

21 Zimmermann, I., Marabelli, A., Bertozzi, C., Sivilotti, L. G. and Dutzler, R. (2012) Inhibition of the Prokaryotic Pentameric Ligand-Gated Ion Channel ELIC by Divalent Cations. PLoS Biol (Clapham, D. E., ed.) **10**, e1001429–14.

22 Tasneem, A., Iyer, L. M., Jakobsson, E. and Aravind, L. (2004) Identification of the prokaryotic ligand-gated ion channels and their implications for the mechanisms and origins of animal Cys-loop ion channels. Genome Biol. **6**, 1–12.

23 Bocquet, N., de Carvalho, L. P., Cartaud, J., Neyton, J., Le Poupon, C., Taly, A., Grutter, T., Changeux, J.-P. and Corringer, P.-J. (2007) A prokaryotic proton-gated ion channel from the nicotinic acetylcholine receptor family. Nature **445**, 116–120.

24 Corringer, P.-J., Poitevin, F., Prevost, M. S., Sauguet, L., Delarue, M. and Changeux, J.-P. (2012) Structure and Pharmacology of Pentameric Receptor Channels: From Bacteria to Brain. Structure/Folding and Design, Elsevier Ltd **20**, 941–956.

25 Smit, A. B., Celie, P. H. N., Kasheverov, I. E., Mordvintsev, D. Y., van Nierop, P., Bertrand, D., Tsetlin, V. and Sixma, T. K. (2006) Acetylcholine-Binding Proteins: Functional and Structural Homologs of Nicotinic Acetylcholine Receptors. J Mol Neurosci **30**, 1–2.

26 Brejc, K., van Dijk, W. J., Klaassen, R. V., Schuurmans, M., van der Oost, J., Schmit, A. B. and Sixma, T. K. (2001) Crystal structure of an ACh-binding protein reveals the ligand-binding domain of nicotinic receptors. Nature **411**, 269–276.

27 Unwin, N. (2005) Refined Structure of the Nicotinic Acetylcholine Receptor at 4Å Resolution. Journal of Molecular Biology **346**, 967–989.

28 Unwin, N. and Fujiyoshi, Y. (2012) Gating Movement of Acetylcholine Receptor Caught by Plunge-Freezing. Journal of Molecular Biology, Elsevier Ltd **422**, 617–634.

29 Morales-Perez, C. L., Noviello, C. M. and Hibbs, R. E. (2016) X-ray structure of the human α4β2 nicotinic receptor. Nature Publishing Group, Nature Publishing Group **538**, 416–416.

30 Zhu, S., Noviello, C. M., Teng, J., Walsh, R. M., Kim, J. J. and Hibbs, R. E. (2018) Structure of a human synaptic GABAA receptor. Nature, Springer US **559**, 67–89.

31 Takai, T., Noda, M., Mishina, M., Shimizu, S., Furutani, Y., Kayano, T., Ikeda, T., Kubo, T., Takahashi, H., Takahashi, T., et al. (1985) Cloning, sequencing and expression of cDNA for a novel subunit of acetylcholine receptor from calf muscle. Nature **315**, 761–765.

32 Lukas, R. J., Changeux, J.-P., Le Novere, N., Albuquerque, E. X., Balfour, D. J. K., Berg, D. K., Bertrand, D., Chiappinelli, V. A., Clarke, P. B. S., Collins, A. C., et al. (1999) International Union of Pharmacology. XX. Current Status of the Nomenclature for Nicotinic Acetylcholine Receptors and Their Subunits. Pharmacological Reviews **51**, 1–5.

33 Lombardo, S. and Maskos, U. (2015) Role of the nicotinic acetylcholine receptor in Alzheimer's disease pathology and treatment. Neuropharmacology, Elsevier Ltd **96**, 255–262.

34 Ghasemi, M. and Hadipour-Niktarash, A. (2015) Pathologic role of neuronal nicotinic acetylcholine receptors in epileptic disorders: implication for pharmacological interventions. Journal of Neuroscience **26**, 199–223.

35 Jurado-Coronel, J. C., Avila-Rodriguez, M., Capani, F., Gonzalez, J., Moran, V. E. and Barreto, G. E. (2016) Targeting the Nicotinic Acetylcholine Receptors (nAChRs) in Astrocytes as a Potential Therapeutic Target in Parkinson's Disease. Current Pharmaceutical Design **22**, 1–7.

36 Fox-Loe, A. M., Dwoskin, L. P. and Richards, C. I. (2016) Nicotinic Acetylcholine

Receptors as Targets for Tobacco Cessation Therapeutics: Cutting-Edge Methodologies to Understand Receptor Assambly and Trafficking. Neuromethods **117**, 119–132.

37 McIntosh, J. M., Santos, A. D. and Olivera, B. M. (1999) Conius Peptides targeted to specific nicotinic acetylcholine receptor subtypes. Annual Reviews Biochemistry **68**, 59–88.

38 Heuser, J. E. and Salpeter, S. R. (1979) Organization of Acetylcholine Receptors in Quick-Frozen, Deep-Etched, and Rotary-Replicated *Torpedo* Postsynaptic Membrane. The Journal of Cell Biology **82**, 150–173.

39 Brisson, A. and Unwin, N. (1984) Tubular Crystalsof Acetylcholine Receptor. The Journal of Cell Biology **99**, 1202–1212.

40 Reynolds, J. A. and Karlin, A. (2002) Molecular weight in detergent solution of acetylcholine receptor from *Torpedo californica*. Biochemistry **17**, 2035–2038.

41 Missias, A. C., Chu, G. C., Klocke, B. J., Sanes, J. R. and Merlie, J. P. (1996) Maturation of the Acetylcholine Receptor in Skeletal Muscle: Regulation of the AChR Gamma-to-Epsilon Switch. Developmental Biology 223–238.

42 Person, A. M., Bills, K. L., Liu, H., Botting, S. K., Lindstrom, J. and Wells, G. B. (2005) Extracellular Domain Nicotinic Acetylcholine Receptors Formed by a4 and b2 Subunits. J. Biol. Chem. **280**, 39990–40002.

43 Lee, W. Y., Free, C. R. and Sine, S. M. (2009) Binding to Gating Transduction in Nicotinic Receptors: Cys-Loop Energetically Couples to Pre-M1 and M2-M3 Regions. Journal of Neuroscience **29**, 3189–3199.

44 Miyazawa, A., Fujiyoshi, Y., Stowell, M. and Unwin, N. (1999) Nicotinic Acetylcholine Receptor at 4.6 AÊ Resolution: Transverse Tunnels in the Channel Wall. Journal of Molecular Biology **288**, 765–786.

45 Hénault, C. M., Sun, J., Therien, J. P. D., daCosta, C. J. B., Carswell, C. L., Labriola, J. M., Juranka, P. F. and Baenziger, J. E. (2015) The role of the M4 lipid-sensor in the folding, trafficking, and allosteric modulation of nicotinic acetylcholine receptors. Neuropharmacology, Elsevier Ltd **96**, 157–168.

46 Hucho, F., Oberthus, W. and Lottspeich, F. (1986) The ion channel of the nicotinic acetylcholine receptor is formed by the homologous helices M II of the receptor subunits. Elsevier **205**, 137–142.

47 Papke, D. and Grosman, C. (2014) The Role of Intracellular Linkers in Gating and Desensitization of Human Pentameric Ligand-Gated Ion Channels. Journal of Neuroscience **34**, 7238–7252.

48 Villarroel, A., Herlitze, S., Koenen, M. and Sakmann, B. (1991) Location of a

threonine residue in the α-subunit M2 transmembrane segment that determines the ion flow through the acetylcholine receptor channel. Proc Natl Acad Sci USA **242**, 69–74.

49 Sullivan, M. P., Owens, J. L. and Kullberg, R. W. (1999) Role of M2 domain residues in conductance and geting of acetylcholine receptors in developing Xenopus muscle. J Physiol **515**, 31–40.

50 Akabas, M. H., Kaufman, C., Archdeacon, P. and Karlin, A. (1994) Identification of Acetylcholine Receptor Channel-Lining Residues in the Entire M2 Segment of the a Subunit. Neuron **13**, 919–927.

51 Chang, Y. and Weiss, D. S. (1998) Substitutions of the Highly Conserved M2 Leucine Create Spontaneously Opening 1 -Aminobutyric Acid Receptors. Molecular Pharmacology 511–523.

52 Stokes, C., Treinin, M. and Papke, R. L. (2015) Looking below the surface of nicotinic acetylcholine receptors. Trends in Pharmacological Sciences, Elsevier Ltd **36**, 514–523.

53 Sine, S. M. (2002) The nicotinic receptor ligand binding domain. J. Neurobiol. **53**, 431–446.

54 Stock, P., Ljaschenko, D., Heckmann, M. and Dudel, J. (2014) Agonists binding nicotinic receptors elicit channel-opening patterns at αγ and αδ sites. J Physiol **592**, 2501–2517.

55 Imoto, K., Busch, C., Sakmann, B., Mishina, M., Konno, T., Nakai, J., Bujo, H., Mori, Y., Fukudo, K. and Numa, S. (1988) Rings of Negatively Charged Amino Acids Determine the Acetylcholine Receptor Channel Conductance. Nature **335**, 645–649.

56 Paas, Y., Gibor, G., Grailhe, R., Savatier-Duclert, N., Dufresne, V., Sunesen, M., de Carvalho, L. P., Changeux, J.-P. and Attali, B. (2005) Pore conformations and gating mechanism of a Cys-loop receptor. PNAS **102**, 15877–15882.

57 Imoto, K., Konno, T., Nakai, J., Want, F., Mishina, M. and Numa, S. (1991) A ring of uncharged polar amino acids as a component of channel constriction in the nicotinic acetylcholine receptor. Elsevier **289**, 193–200.

58 Hodgkin, A. L. and Huxley, A. F. (1951) Currents Carried by Sodium and Potassium Ions through the membrane of the Giant Axon of *Loligo*. J Physiol **II6**, 449–472.

59 Neher, E. and Sakmann, B. (1976) Single-channel currents recorded from membrane of denerved frog muscle fibres. Nature 799–803.

60 Priel, A., Gil, Z., Moy, V. T., Magleby, K. L. and Silberberg, S. D. (2007) Ionic

Requirements for Membrane-Glass Adhesion and Giga Seal Formation in Patch-Clamp Recording. Biophysical Journal **92**, 3893–3900.

61 Cox, D. R. and Miller, H. D. (1965) The Theory of Stochastic Processes. Chapman HallCRC.

62 Hamill, O. P., Marty, A., Neher, E., Sakmann, B. and Sigworth, F. J. (1981) Improved Patch-Clamp Techniques for High-Resolution Current Recording from Cells and Cell-Free Membrane Patches. European Journal of Phyisology **391**, 85–100.

63 Del Castillo, J. and Katz, B. (1957) Interaction at end-plate receptors between different choline derivatives. The Royal Society **146**, 369–381.

64 Gupta, S., Charaborty, S., Vij, R. and Auerbach, A. (2016) A mechanism for acetylcholine receptor gating based on structure, coupling, phi, and flip. J. Gen. Physiol. **149**, 85–103.

65 Purohit, P. and Auerbach, A. (2007) Acetylcholine Receptor Gating at Extracellular Transmembrane Domain Interface: the "Pre-M1" Linker. J. Gen. Physiol. **130**, 559–568.

66 Lape, R., Krashia, P., Colquhoun, D. and Sivilotti, L. G. (2009) Agonist and blocking actions of choline and tetramethylammonium on human muscle acetylcholine receptors. J Physiol **587**, 5045–5072.

67 Sine, S. M. and Steinbach, J. H. (1984) Agonsits Block Currents Through Acetylcholine Receptor Channels. Biophysical Journal **46**, 227–284.

68 Hilf, R. J. C., Bertozzi, C., Zimmermann, I., Reiter, A., Trauner, D. and Dutzler, R. (2010) Structural basis of open channel block in a prokaryotic pentameric ligand-gated ion channel. Nature Structural & Molecular Biology, Nature Publishing Group **17**, 1330–1336.

69 Maconochie, D. J. and Steinbach, J. H. (1995) Block by Acetylcholine of Mouse Muscle Nicotinic Receptors, StablyExpressed in Fibroblasts. J. Gen. Physiol. **106**, 113–147.

70 Monod, J., Wyman, J. and Changeux, J.-P. (1965) On the nature of allosteric transitions: A plausible model. Journal of Molecular Biology, Academic Press Inc. (London) Ltd. **12**, 88–118.

71 Lape, R., Colquhoun, D. and Sivilotti, L. G. (2008) On the nature of partial agonism in the nicotinic receptor superfamily. Nature **547**, 729–18.

72 Mukhtasimova, N., Lee, W. Y., Wang, H.-L. and Sine, S. M. (2009) Detection and trapping of intermediate states priming nicotinic receptor channel opening. Nature, Nature Publishing Group **459**, 451–454.

73 Katz, B. and Thesleff, S. (1957) A Study of the "Desensitization" Produced by Acetylcholine at the Motor End-Plate. J Physiol 63–80.

74 Bouzat, C. B., Andersen, N. D., Corradi, J. and Sine, S. M. (2012) Contribution of Agonist Binding Sites and Coupling Regions to Activation and Desensitization of Homomeric Cys-Loop Receptors. Biophysical Journal **102**, 418a–2.

75 Colquhoun, D. and Lape, R. (2012) Allosteric coupling in ligand-gated ion channels. J. Gen. Physiol., Rockefeller University Press **140**, 599–612.

76 Hanson-Smith, V., Kolaczkowski, B. and Thornton, J. W. (2010) Robustness of Ancestral Sequence Reconstruction to Phylogenetic Uncertainty. Molecular Biology and Evolution **27**, 1988–1999.

77 Finnigan, G. C., Hanson-Smith, V., Stevens, T. H. and Thornton, J. W. (2012) Evolution of increased complexity in a molecular machine. Nature, Nature Publishing Group **481**, 394–398.

78 Sheng, M. and Pak, D. T. S. (2000) Ligand-gated ion channel interactions with cytoskeletal and signaling proteins. Physiological Reviews **62**, 755–778.

79 Edgar, R. C. (2004) MUSCLE: multiple sequence alignment with high accuracy and high throughput. Nucleic Acids Research **32**, 1792–1797.

80 Veidenberg, A., Medlar, A. and Löytynoja, A. (2016) Wasabi: An Integrated Platform for Evolutionary Sequence Analysis and Data Visualization. Molecular Biology and Evolution **33**, 1126–1130.

81 Löytynoja, A. and Goldman, N. (2005) An algorithm for progressive multiple alignment of sequences with insertions. PNAS **102**, 10557–10562.

82 Abascal, F., Zardoya, R. and Posada, D. (2005) ProtTest: selection of best-fit models of protein evolution. Bioinformatics **21**, 2104–2105.

83 Guindon, S., Dufayard, J.-F., Lefort, V., Anisimova, M., Hordijk, W. and Gascuel, O. (2010) New Algorithms and Methods to Estimate Maximum-Likelihood Phylogenies: Assessing the Performance of PhyML 3.0. Systematic Biology **59**, 307–321.

84 Anisimova, M. and Gascuel, O. (2006) Approximate Likelihood-Ratio Test for Branches: A Fast, Accurate, and Powerful Alternative. Systematic Biology (Sullivan, J., ed.) **55**, 539–552.

85 Xu, B. and Yang, Z. (2013) PAMLX: A Graphical User Interface for PAML. Molecular Biology and Evolution **30**, 2723–2724.

86 Fitch, W. M. and Smith, T. F. (1983) Optimal sequence alignments. Proc Natl Acad Sci USA **80**, 1382–1386.

87 Prinston, J. E., Emlaw, J. R., Dextraze, M. F., Tessier, C. J. G., Pérez-Areales, F. J., McNulty, M. S. and daCosta, C. J. B. (2017) Ancestral Reconstruction Approach to Acetylcholine Receptor Structure and Function. Structure/Folding and Design, Elsevier Ltd. **25**, 1295–1302.e3.

88 Pear, W. S., Nolan, G. P., Scott, M. L. and Baltimore, D. (1993) Production of high-titer helper-free retroviruses by transient transfection. Proc Natl Acad Sci USA **90**, 8392–8397.

89 Mukhtasimova, N., daCosta, C. J. B. and Sine, S. M. (2016) Improved resolution of single channel dwell times reveals mechanisms of binding, priming, and gating in muscle AChR. J. Gen. Physiol. **148**, 43–63.

90 Rayes, D., De Rosa, M. J., Sine, S. M. and Bouzat, C. (2009) Number and Locations of Agonist Binding Sites Required to Activate Homomeric Cys-Loop Receptors. Journal of Neuroscience **29**, 6022–6032.

91 Sachs, F. and Barkakati, N. (1982) The Automated Analysis of data from Single Ionic Channels. European Journal of Phyisology 331–340.

92 Auerbach, A. and Sachs, F. (1983) Flickering of a nicotinic ion channel to a subconductance state. Biophysj, Elsevier **42**, 1–10.

93 Auerbach, A. and Sachs, F. (1984) Single-channel currents from acetylcholine receptors in embryonic chick muscle. Kinetic and conductance properties of gaps within bursts. Biophysj, Elsevier **45**, 187–198.

94 Gration, K., Lambert, J. J., Ramsey, R. L., Rand, R. P. and Usherwood, P. N. R. (1982) Closure of membrane channels gated by glutamate receptors may be a two-step process. Nature **295**, 1–3.

95 Sakmann, B. and Neher, E. (2009) Single-Channel Recording, Second Edition 1–705.

96 Sigworth, F. J. and Sine, S. M. (1987) Data transformations for improved display and fitting of single-channel dwell time histograms. Biophysj, Elsevier **52**, 1047–1054.

97 van der Loo, M. P. J. (2010) Distribution based outlier detection in univariate data. Statistics Netherlands 1–14.

98 Qin, F., Auerbach, A. and Sachs, F. (1996) Estimating Single-Channel Kinetic Parameters from Idealized Patch-Clamp Data Containing Missed Events. Biophysical Journal **70**, 264–280.

99 Chen, Q., Kinde, M. N., Arjunan, P., Wells, M. M., Cohen, A. E., Xu, Y. and Tang, P. (2015) Direct Pore Binding as a Mechanism for Isoflurane Inhibition of the Pentameric Ligand-gated Ion Channel ELIC. Nature Publishing Group, Nature

Publishing Group 1–11.

100 Imoto, K., Methfessek, C., Sakmann, B., Mishina, M., Mori, Y., Konno, T., Fuduka, K., Kurasaki, M., Bujo, H., Fujita, Y., et al. (1986) Location of a delta-subunit region determining ion transport through the acetylcholine receptor channel. Nature **324**, 670–674.

101 Villarroel, A., Herlitze, S., Witzmann, V., Koenen, M. and Sakmann, B. (1992) Asymmetry of the rat acetylcholine receptor subunits in the narrow region of the pore. Proc Natl Acad Sci USA **249**, 317–324.

102 Charnet, P., Labarca, C., Leonard, R. J., Vogelaar, N. J., Czyzyk, L., Gouin, A., Davidson, N. and Lester, H. A. (1990) An Open-Channel Blocker Interacts with Adjacent Turns of a-Helices in the Nicotinic Acetylcholine Receptor. Neuron **2**, 87–95.

103 Kim, S., Chamberlain, A. K. and Bowie, J. U. (2004) A Model of the Closed Form of the Nicotinic Acetylcholine Receptor M2 Channel Pore. Biophysical Journal **87**, 792–799.

104 Tessier, C. J. G., Emlaw, J. R., Cao, Z. Q., Pérez-Areales, F. J., Salameh, J.-P. J., Prinston, J. E., McNulty, M. S. and daCosta, C. J. B. (2017) Back to the future: Rational maps for exploring acetylcholine receptor space and time. BBA - Proteins and Proteomics, Elsevier **1865**, 1522–1528.

SECTION 8.0: SUPPLEMENTAL INFORMATION

APPENDIX I:

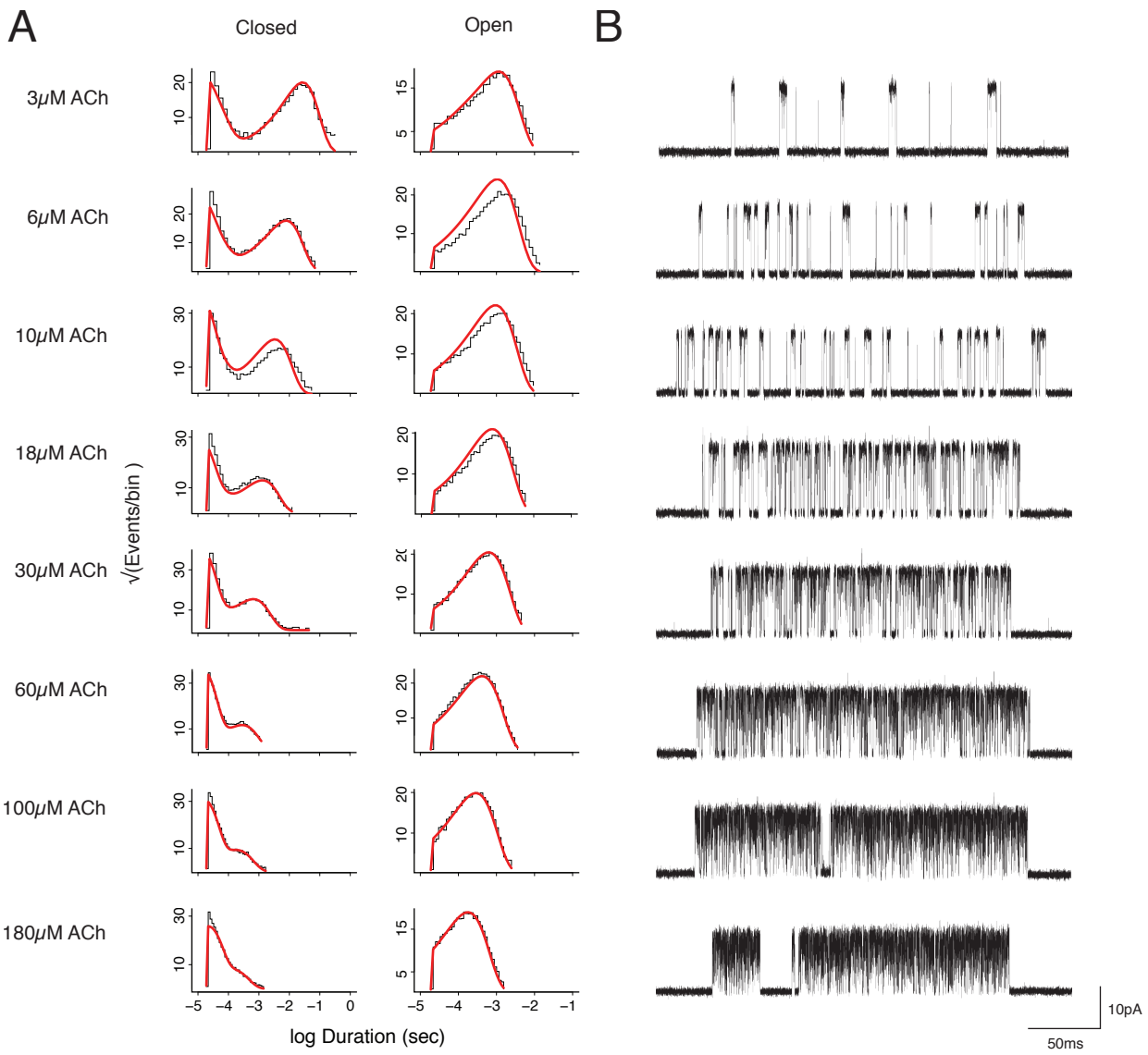

Supplemental figure 1: Duplicate single-channel analysis of wild type (WT) receptors. **(A)** For each of the denoted acetylcholine (ACh) concentrations, closed and open dwell time histograms are displayed on a log axis, with the global fit of the del Castillo and Katz kinetic scheme (Scheme I) overlaid. Rate constants for global fit data are displayed in Table 1. (B) Ancestral $\beta_{Anc}84$ subunit was combined with *Homo sapiens*, α, ϵ and δ wild type subunits. Acetylcholine elicited single-channel recordings obtained as described in Materials and Methods 3.5-3.6.

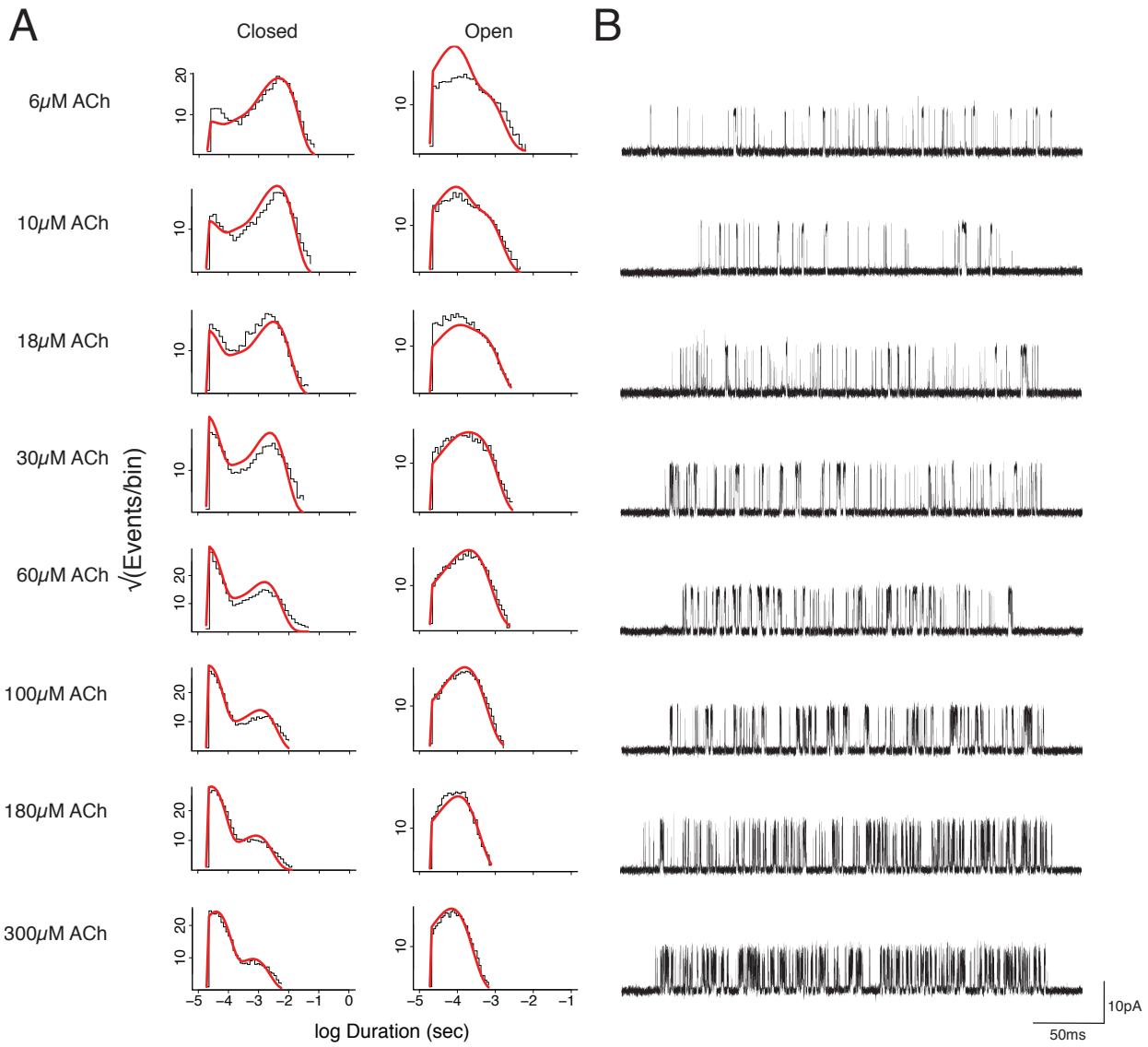

Supplemental figure 2: Duplicate single-channel analysis of $\beta_{Anc}81$ containing receptors.
(A) For each of the denoted acetylcholine (ACh) concentrations, closed and open dwell time histograms are displayed on a log axis, with the global fit of the del Castillo and Katz kinetic scheme (Scheme I) overlaid. Rate constants for global fit data are displayed in Table 1. (B) Ancestral $\beta_{Anc}81$ subunit was combined with *Homo sapiens*, α, ϵ and δ wild type subunits. Acetylcholine elicited single-channel recordings obtained as described in Materials and Methods 3.5-3.6.

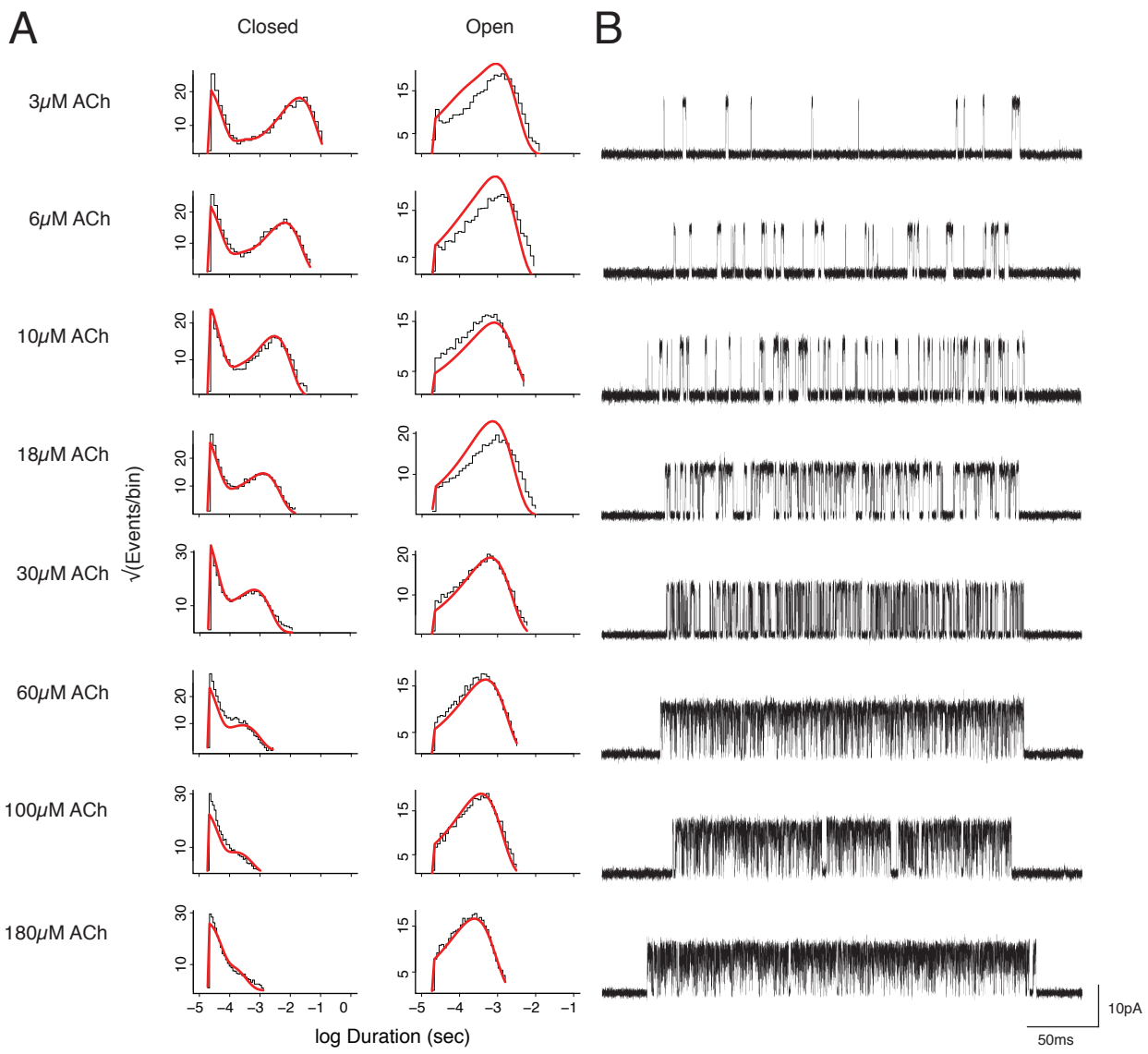

Supplemental figure 3: Duplicate single-channel analysis of $\beta_{Anc}84$ containing receptors.
(A) For each of the denoted acetylcholine (ACh) concentrations, closed and open dwell time histograms are displayed on a log axis, with the global fit of the del Castillo and Katz kinetic scheme (Scheme I) overlaid. Rate constants for global fit data are displayed in Table 1. (B) Ancestral $\beta_{Anc}84$ subunit was combined with *Homo sapiens*, α, ϵ and δ wild type subunits. Acetylcholine elicited single-channel recordings obtained as described in Materials and Methods 3.5-3.6.

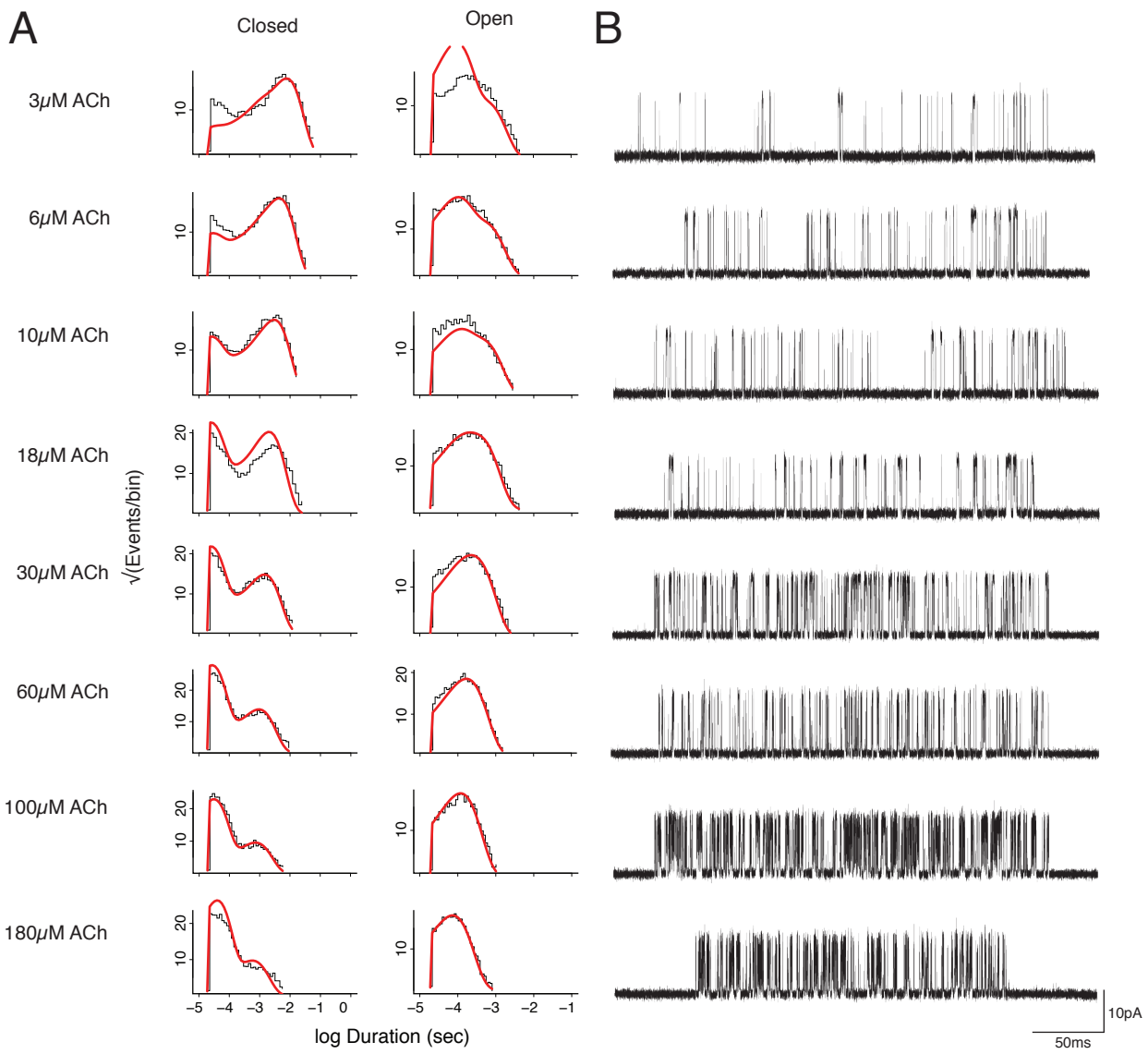

Supplemental figure 4: Duplicate single-channel analysis of β_{Anc}81 T2'G receptors
(A) For each of the denoted acetylcholine (ACh) concentrations, closed and open dwell time histograms are displayed on a log axis, with the global fit of the del Castillo and Katz kinetic scheme (Scheme I) overlaid. Rate constants for global fit data are displayed in Table 1. (B) Ancestral β_{Anc}81 T2'G subunit was combined with *Homo sapiens*, α, ϵ and δ wild type subunits. Acetylcholine elicited single-channel recordings obtained as described in Materials and Methods 3.5-3.6.

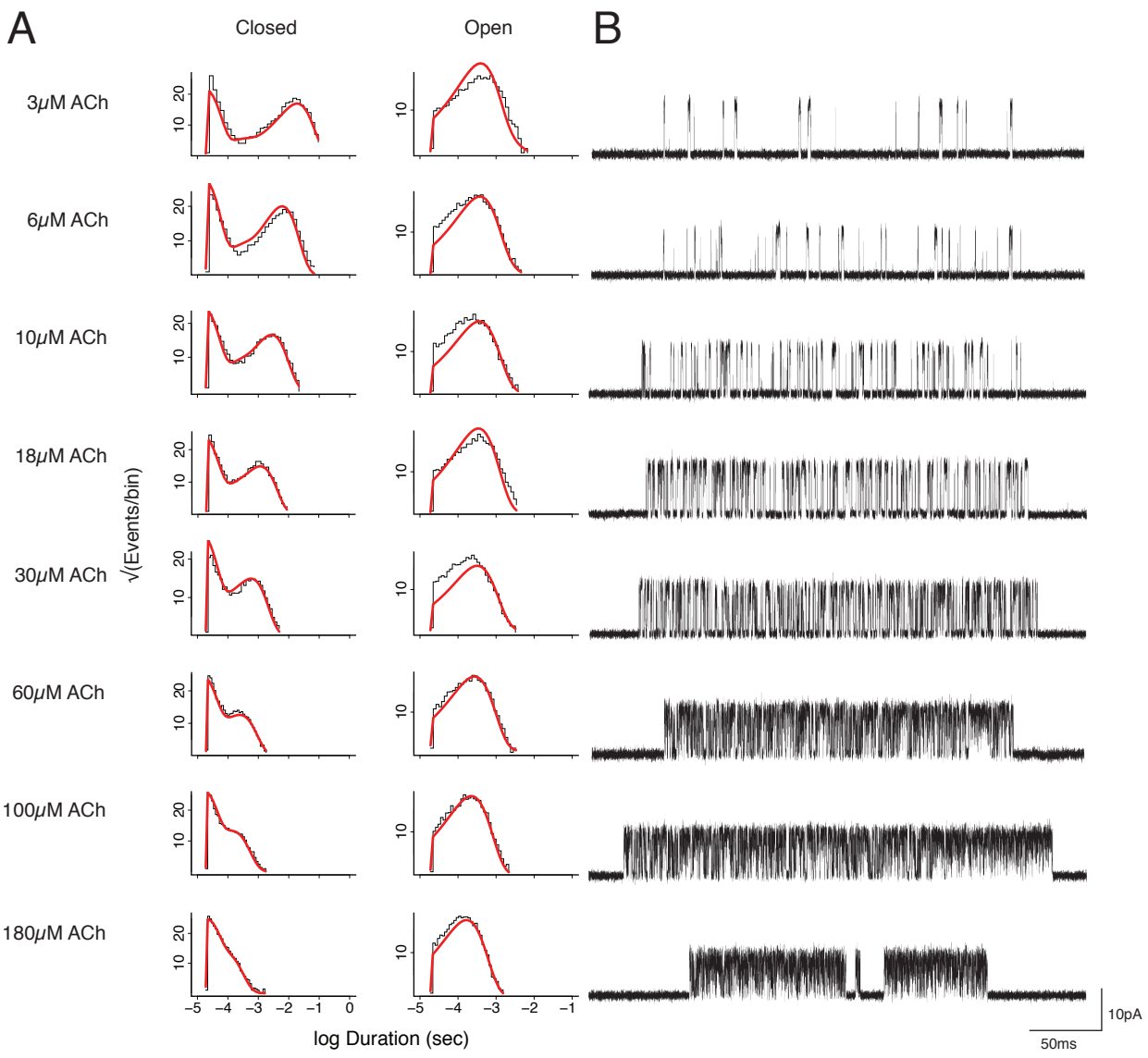

Supplemental figure 5: Duplicate single-channel analysis of β_{Anc}81 S6'F receptors.
(A) For each of the denoted acetylcholine (ACh) concentrations, closed and open dwell time histograms are displayed on a log axis, with the global fit of the del Castillo and Katz kinetic scheme (Scheme I) overlaid. Rate constants for global fit data are displayed in Table 1. (B) Ancestral β_{Anc}81 S6'F subunit was combined with *Homo sapiens*, α, ϵ and δ wild type subunits. Acetylcholine elicited single-channel recordings obtained as described in Materials and Methods 3.5-3.6.

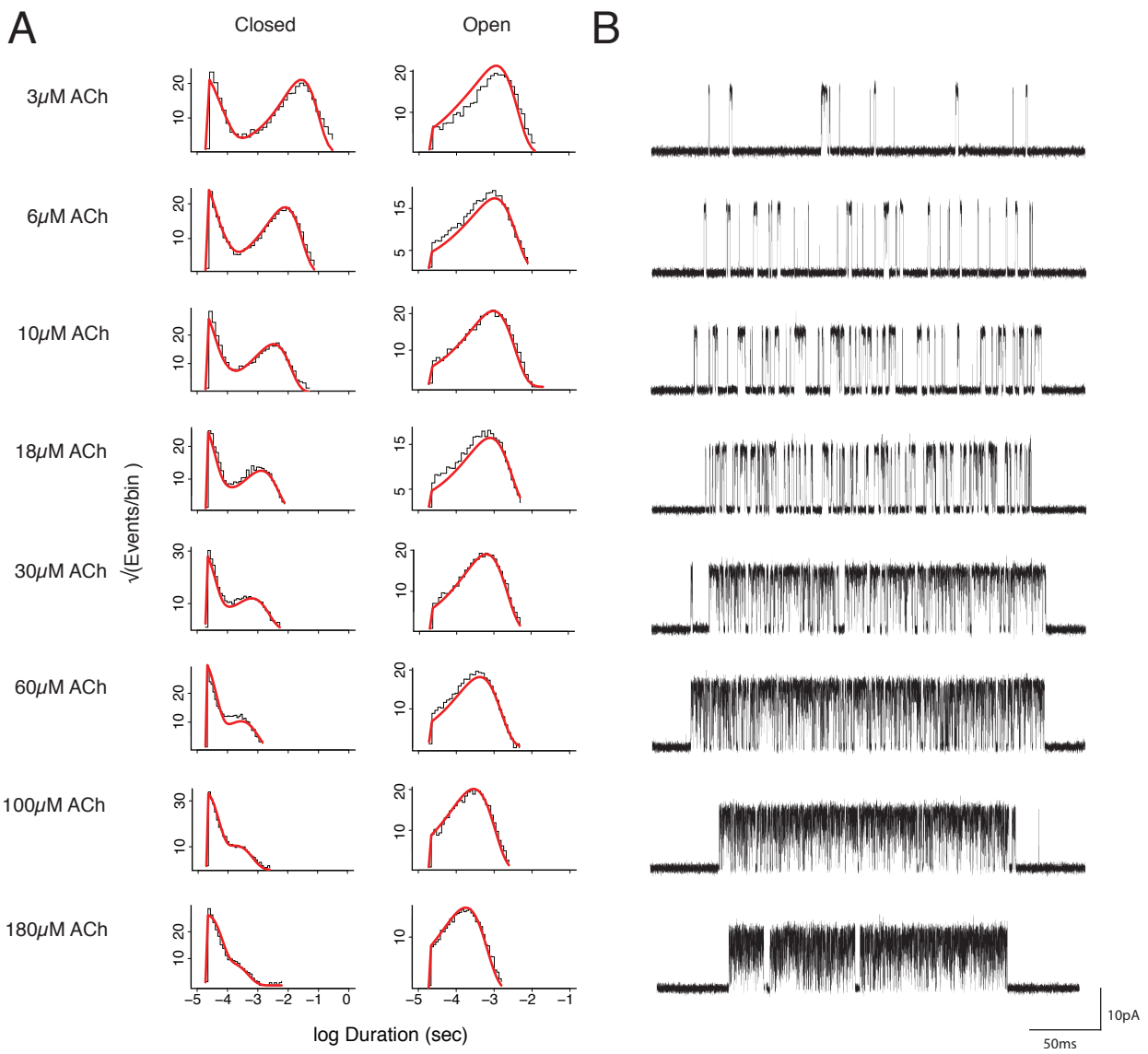

Supplemental figure 6: Triplicate single-channel analysis of wild type (WT) receptors.
(A) For each of the denoted acetylcholine (ACh) concentrations, closed and open dwell time histograms are displayed on a log axis, with the global fit of the del Castillo and Katz kinetic scheme (Scheme I) overlaid. Rate constants for global fit data are displayed in Table 1. (B) Ancestral $\beta_{Anc}84$ subunit was combined with *Homo sapiens*, α, ϵ and δ wild type subunits. Acetylcholine elicited single-channel recordings obtained as described in Materials and Methods 3.5-3.6.

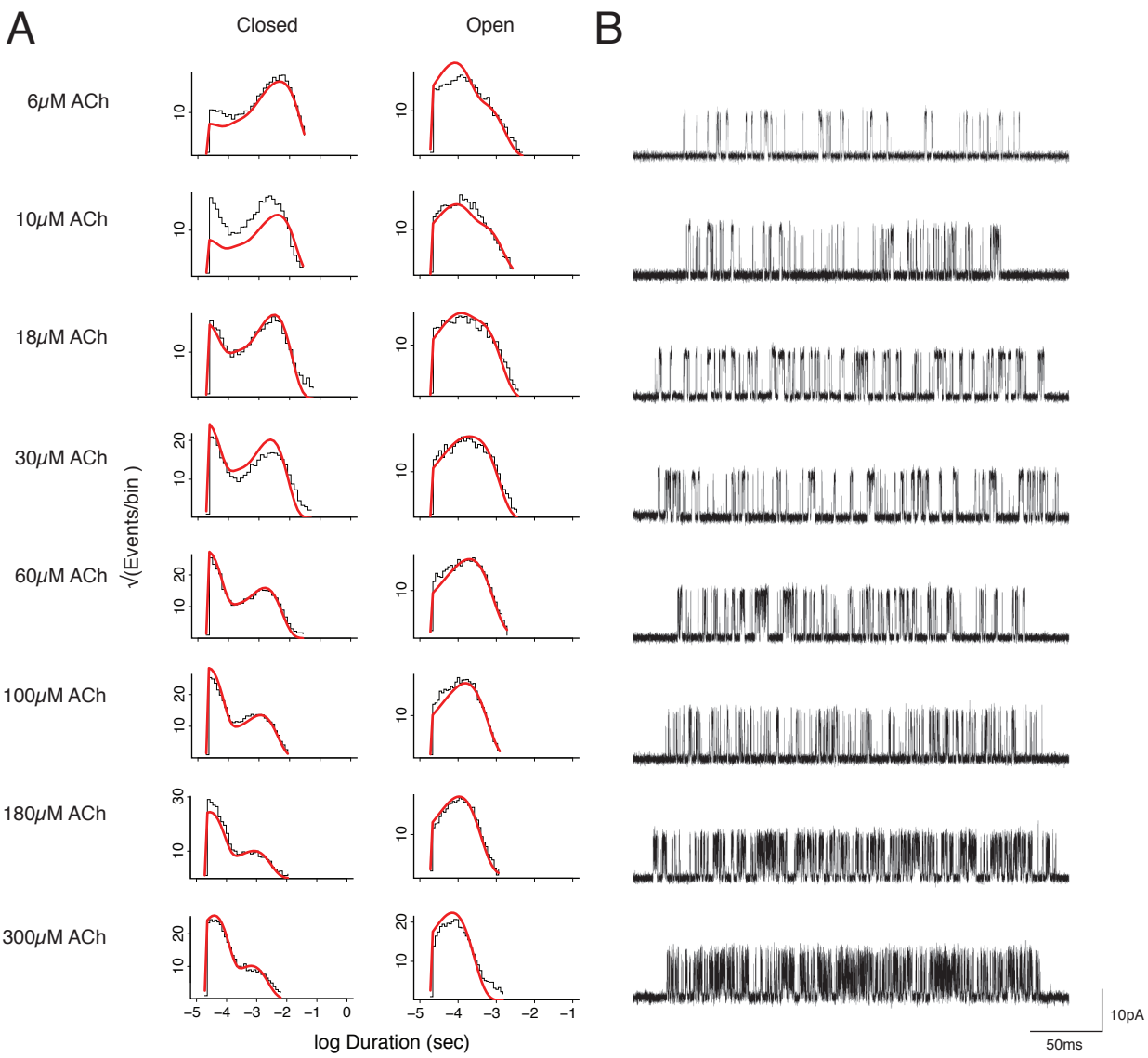

Supplemental figure 7: Triplicate single-channel analysis of $\beta_{Anc}81$ containing receptors. **(A)** For each of the denoted acetylcholine (ACh) concentrations, closed and open dwell time histograms are displayed on a log axis, with the global fit of the del Castillo and Katz kinetic scheme (Scheme I) overlaid. Rate constants for global fit data are displayed in Table 1. (B) Ancestral $\beta_{Anc}81$ subunit was combined with *Homo sapiens*, α, ϵ and δ wild type subunits. Acetylcholine elicited single-channel recordings obtained as described in Materials and Methods 3.5-3.6.

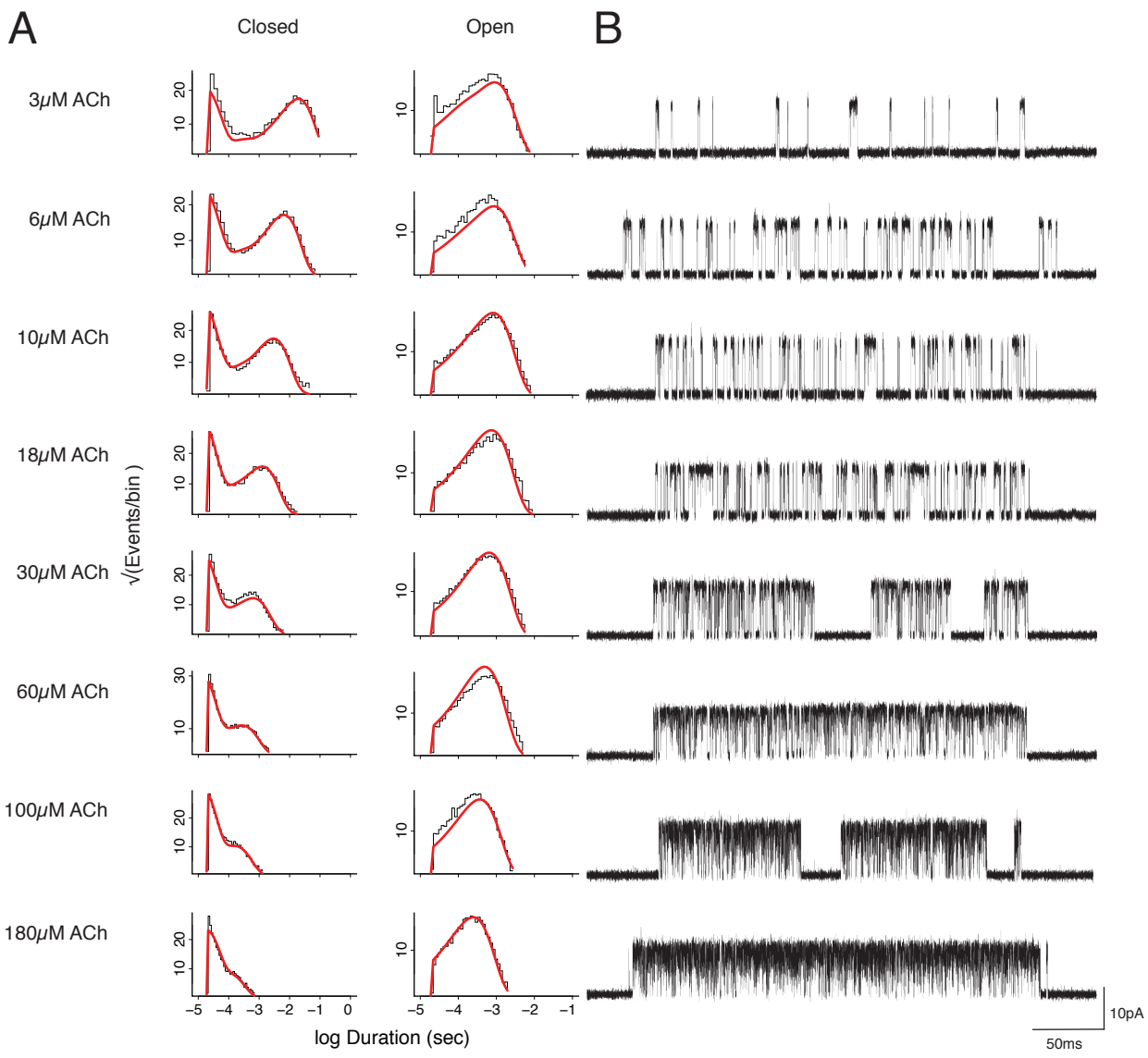

Supplemental figure 8: Triplicate single-channel analysis of $\beta_{Anc}84$ containing receptors.
(A) For each of the denoted acetylcholine (ACh) concentrations, closed and open dwell time histograms are displayed on a log axis, with the global fit of the del Castillo and Katz kinetic scheme (Scheme I) overlayed. Rate constants for global fit data are displayed in Table 1. (B) Ancestral $\beta_{Anc}84$ subunit was combined with *Homo sapiens*, α, ϵ and δ wild type subunits. Acetylcholine elicited single-channel recordings obtained as described in Materials and Methods 3.5-3.6.

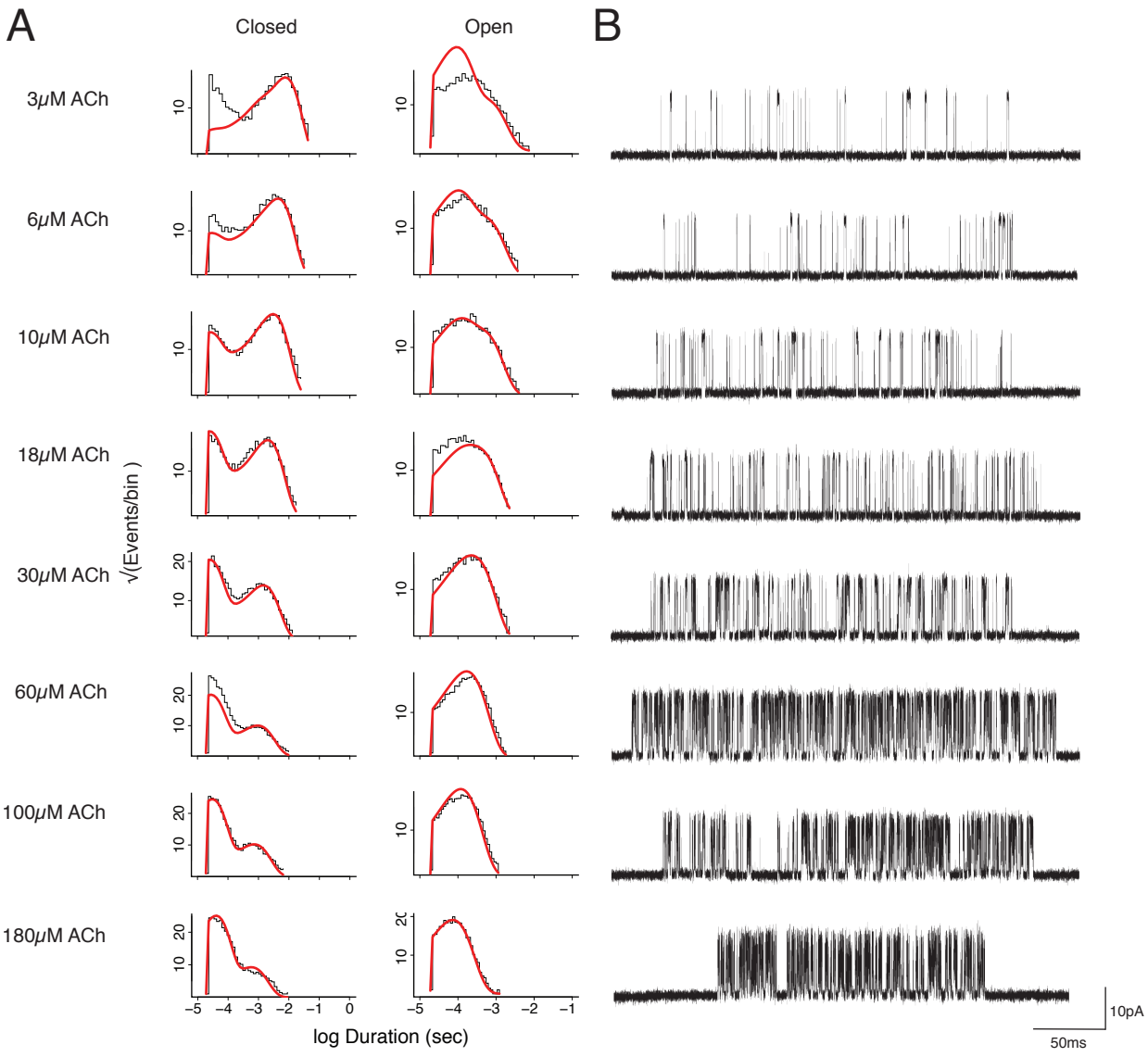

Supplemental figure 9: Triplicate single-channel analysis of β_{Anc}81 T2'G receptors
(A) For each of the denoted acetylcholine (ACh) concentrations, closed and open dwell time histograms are displayed on a log axis, with the global fit of the del Castillo and Katz kinetic scheme (Scheme I) overlaid. Rate constants for global fit data are displayed in Table 1. (B) Ancestral β_{Anc}81 T2'G subunit was combined with *Homo sapiens*, α, ϵ and δ wild type subunits. Acetylcholine elicited single-channel recordings obtained as described in Materials and Methods 3.5-3.6.

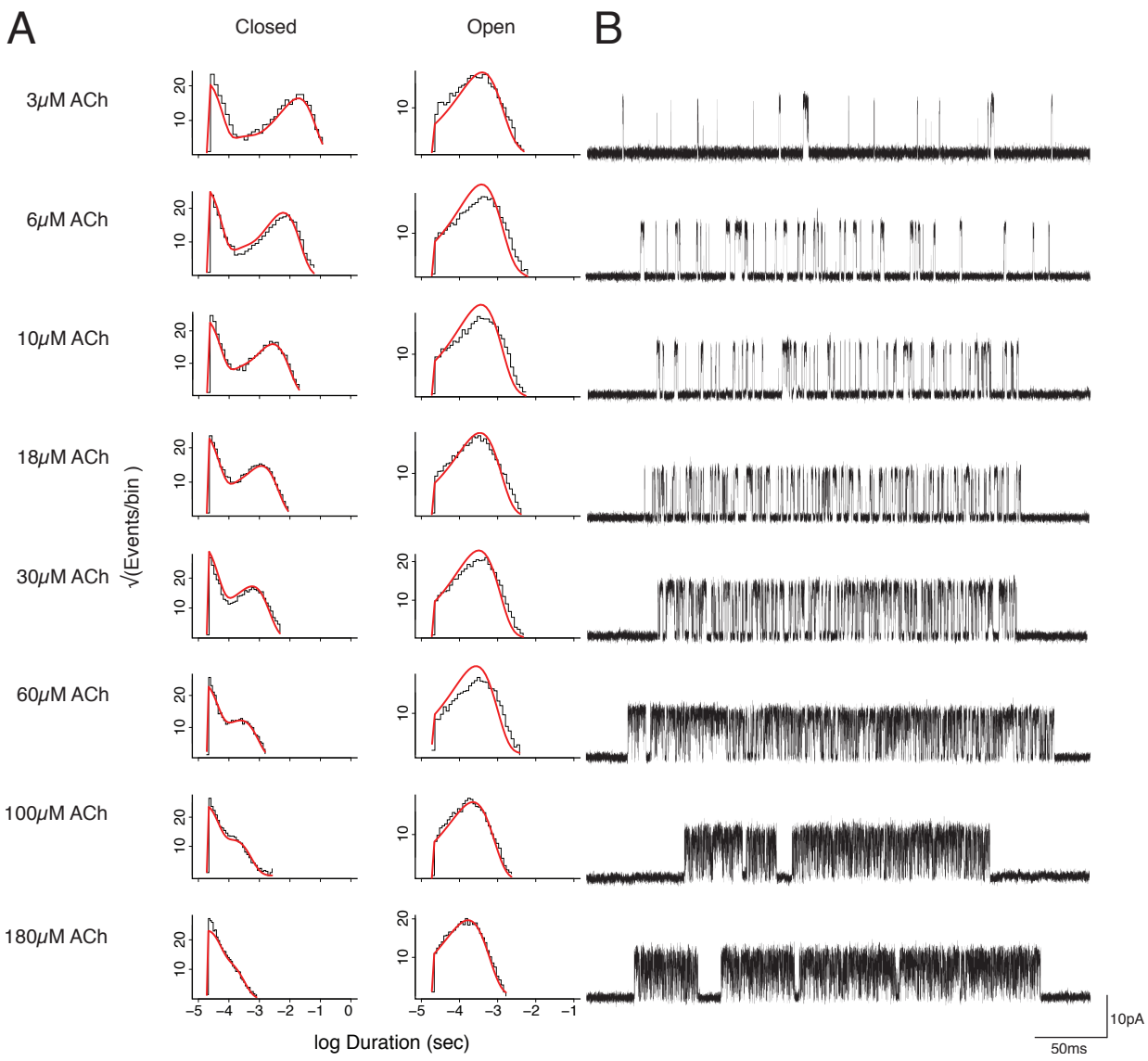

Supplemental figure 10: Triplicate single-channel analysis of β_{Anc}81 S6'F receptors.
(A) For each of the denoted acetylcholine (ACh) concentrations, closed and open dwell time histograms are displayed on a log axis, with the global fit of the del Castillo and Katz kinetic scheme (Scheme I) overlaid. Rate constants for global fit data are displayed in Table 1. (B) Ancestral β_{Anc}81 S6'F subunit was combined with *Homo sapiens*, α, ϵ and δ wild type subunits. Acetylcholine elicited single-channel recordings obtained as described in Materials and Methods 3.5-3.6.

Supplemental table 1: Kinetics of muscle type AChR- activation by acetylcholine
Single-channel kinetic rates of wild type receptors, and receptors containing denoted ancestral β subunit with complementary wild type subunits. Binding and gating rates and errors were computed by MIL software. The channel gating equilibrium constants $\Theta=\beta_n/\alpha_n$ and the dissociation constant $K = k_{-1}/k_{+1}$. Example of error propagation calculation or equilibrium constants provided in supplemental information.

Binding	Wild Type	βAnc84	βAnc81 S6'F	βAnc81 T2'G	βAnc81
k+1	651.5 ± 34.3	317.41 ± 8.77	303.84 ± 5.82	189.05 ± 4.61	72.37 ± 1.37
k-1	14380.18 ± 1010.73	4097.88 ± 137.76	3518.17 ± 110.93	660.46 ± 51.82	140.69 ± 9.84
K1 (μM)	22 ± 1.93	13 ± 0.566	11.6 ± 0.428	3 ± 0.246	2 ± 0.145
k+2	325.75 ± 17.13	158.71 ± 4.38	151.92 ± 2.91	94.53 ± 2.30	36.18 ± 0.69
k-2	26452 ± 407.51	27271.18 ± 239.47	23917.64 ± 173.41	8463.46 ± 218.61	6450.83 ± 189.92
K2 (μM)	81 ± 4.45	172 ± 4.98	158 ± 3.22	90 ± 3.18	179 ± 6.25
k+b	213.60 ± 3.15	172.27 ± 3.88	157.43 ± 4.53	186.13 ± 1.51	157.52 ± 1.98
k-b	106568.66 ± 802.06	120083.07 ± 1191.72	108321.12 ± 1499.34	51620.10 ± 430.27	68605.30 ± 686.68
Kb (μM)	500 ± 8.26	698 ± 17.16	688 ± 21.97	277 ± 3.23	435 ± 7.00

Gating	Wild Type	βAnc84	βAnc81 S6'F	βAnc81 T2'G	βAnc81
β1	33.18 ± 2.41	76.95 ± 2.96	31.54 ± 2.69	397.00 ± 9.46	296.35 ± 4.18
α1	8756.74 ± 651.07	10436.91 ± 407.74	1284.39 ± 34.79	12948.20 ± 446.16	14835.54 ± 398.17
Θ1	0.0038 ± 0.00039	0.0074 ± 0.0004	0.025 ± 0.0022	0.031 ± 0.0013	0.02 ± 0.0006
β2	14146.65 ± 448.18	34706 ± 708.53	41814.48 ± 623.22	2946.58 ± 94.90	2893.54 ± 87.23
α2	1079.81 ± 10.45	1887.00 ± 21.92	5122 ± 56.90	1972.57 ± 19.50	2312.10 ± 17.77
Θ2	13.1 ± 0.434	18.4 ± 0.432	8.2 ± 0.152	1.5 ± 0.050	1.3 ± 0.039

Error Propagation calculation. (Example provided from Wild type K_1)

WT: $k_{+1} = 651.5 \pm 34.3$
$k_{-1} = 14380.18 \pm 1010.73$
$K_1 = 22 \pm ???$

$$\frac{\Delta z}{z} = \sqrt{\left(\frac{\Delta x}{cx}\right)^2 + \left(\frac{\Delta y}{y}\right)^2}$$

$$\frac{\Delta z}{22} = \sqrt{\left(\frac{1010.73}{14380.18}\right)^2 + \left(\frac{34.3}{651.5}\right)^2}$$

$$\frac{\Delta z}{22} = \sqrt{0.007711951}$$

$$\Delta z = 0.087817715 * 22 = 1.93$$